Viscous potential flow analysis of Kelvin-Helmholz instability in a channel

by T. Funada and D.D. Joseph
University of Minnesota
September 2000
file: DDJ/2000/papers/khinstab-L.tex printed November 3, 2000

Abstract
We study the stability of stratified gas-liquid flow in a horizontal rectangular channel using viscous potential flow. The analysis leads to an explicit dispersion relation in which the effects of surface tension and viscosity on the normal stress are not neglected but the effect of shear stresses are neglected. Formulas for the growth rates, wave speeds and neutral stability curve are given in general and applied to experiments in air-water flows. The effects of surface tension are always important and actually determine the stability limits for the cases in which the volume fraction of gas is not too small. The stability criterion for viscous potential flow is expressed by a critical value of the relative velocity. The maximum critical value is when the viscosity ratio is equal to the density ratio; surprisingly the neutral curve for this viscous fluid is the same as the neutral curve for inviscid fluids. The maximum critical value of the velocity overall viscous fluids is given by inviscid fluids. For air at 20°C and liquids with density $\rho = 1g/cc$ the liquid viscosity for the critical conditions is 15 cp; the critical velocity for liquids with viscosities larger than 15 cp are only slightly smaller but the critical velocity for liquids smaller than 15 cp, like water, can be much lower. The viscosity of the liquid has a strong affect on the growth rate. The viscous potential flow theory fits the experimental data for air and water well for liquid and water when the gas fraction is greater than about 70%.

1 Introduction

It is well known that the Navier-Stokes equations are satisfied by potential flow; the viscous term is identically zero when the vorticity is zero but the viscous stresses are not zero (Joseph and Liao [JL] 1994). It is not possible to satisfy the no-slip condition at a solid boundary or the continuity of the tangential component of velocity and shear stress at a fluid-fluid boundary when the velocity is given by a potential. The viscous stresses enter into the viscous potential flow analysis of free surface problems through the normal stress balance (2.20) at the interface. Viscous potential flow analysis gives good approximations to fully viscous flows in cases where the shears from the gas flow are negligible; the Rayleigh-Plesset bubble is a potential flow which satisfies the Navier-Stokes equations and all the interface conditions. Joseph, Belanger and Beavers [JBB] 1999 constructed a viscous potential flow analysis of the Rayleigh-Taylor instability which can scarcely be distinguished from the exact fully viscous analysis.

The success of viscous potential flow in the analysis of Rayleigh-Taylor instability has motivated the analysis of Kelvin-Helmholz theory given here and in the recent short paper by Joseph, Lundgren and Funada [JLF] 2000. The JLF paper treats the Kelvin-Helmhohlz instability problem of two adjacent streams with different speed in fluids with different viscosities when surface tension is neglected. It is well known that the instability that arises when surface tension and viscosity are neglected is catastrophic; short waves with wave lengths $\lambda = 2\pi/k$ amplify without control like e^{kt}. The instability grows exponentially as the wavenumber $k \to \infty$ no matter how small time t. This kind of catastrophic instability is called Hadamard instability (Joseph and Saut [JS] 1990). In the case of inviscid fluids

this instability is regularized by surface tension which stabilizes the short waves; surface tension is very important.

The question addressed in the paper by Joseph, Lundgren and Funada 2000 is whether viscosity, without surface tension, would regularize the Hadamard instability. The answer depends on what 'regularize' is. Unlike surface tension, viscosity will not cause the small waves to decay; they still grow but their growth is limited and the growth rate $re\sigma(k)$ does not go to infinity with k as in Hadamard instability. An explicit formula for the growth rates for short waves was given; the positive growth rate is given by

$$re\sigma_+ = \frac{\rho_a\mu_l^2 + \rho_l\mu_a^2}{2\left(\mu_l + \mu_a\right)^3}\left(U_a - U_l\right)^2 \quad k \to \infty$$

where $[\rho, \mu, U] = [density, viscosity, velocity]$.

The present paper gives a detailed report of the viscous potential flow analysis of KH instability in a rectangular duct together with a comparison of theory and experiment in the case of air-water flow. As we have already mentioned potential flow requires that we neglect the no-slip condition at solid surfaces. In the rectangular channel the top and bottom walls are perpendicular to gravity; the bottom wall is under the liquid and parallel to the undisturbed uniform stream; the top wall contacts gas only. The side walls are totally inactive; there is no motion perpendicular to the side walls unless it is created initially and since the two fluids slip at the walls all the conditions required in the analysis of three dimensions can be satisfied by flow in two dimensions which is analyzed here.

The viscosity in viscous potential flow enters into the normal stress balance rather than tangential stress balance. Air over liquid induces small viscous stresses that may be confined to boundary layer and may be less and less important as the viscosity of the liquid increases. At a flat, free surface $z = 0$ with velocity components (u, w) corresponding to (x, z) the shear stress is given by

$$\mu\left(\frac{\partial u}{\partial z} + \frac{\partial w}{\partial x}\right)$$

and the normal stress is

$$2\mu\frac{\partial w}{\partial z}.$$

The normal stress is an extensional rather than a shear stress and it is activated by waves on the liquid; the waves are induced more by pressure than by shear. For this reason, we could argue that the neglect of shear could be justified in wave motions in which the viscous resistance to wave motion is not negligible; this is the situation which may be well approximated by viscous potential flow.

2 Formulation of the problem

A channel of rectangular cross section with height H and width W and of length L is set horizontally, in which a gas layer is over a liquid layer: the two-layer Newtonian incompressible fluids are immiscible. The undisturbed interface is taken at $z = 0$ with the z-axis of Cartesian coordinates $\boldsymbol{x} = (x, y, z) = (x_1, x_2, x_3)$, where $0 \le x \le L$, $0 \le y \le W$, and $-h_l \le z \le h_a$ $(H = h_l + h_a)$; acceleration due to gravity $\boldsymbol{g} = (0, 0, -g)$. We denote velocity by $\boldsymbol{v} = (u, v, w) = (v_1, v_2, v_3)$, pressure p, density ρ, viscosity μ, viscous stress tensor τ or τ_{ij} (in the conventional tensor notation), strain tensor e or e_{ij}, interface elevation h, surface tension γ.

In the undisturbed state, the gas (air) with a uniform flow $(U_a, 0, 0)$ is in $0 < z < h_a$, and the liquid with a uniform flow $(U_l, 0, 0)$ is in $-h_l < z < 0$; the pressure has an equilibrium distribution due to the gravity. We consider Kelvin-Helmholz instability of small disturbances against the undisturbed state.

The perscription of a discontinuity in velocity across $z = 0$ is not compatible with the no-slip condition of Navier-Stokes viscous fluid mechanics. The discontinuous prescription of data in the study of Kelvin-Helmholz instability is a viscous potential flow solution of the Navier-Stokes in which no-slip conditions at walls and no slip and continuity of shear stress across the gas liquid interface are neglected. Usually the analysis

of Kelvin-Helmholz instability is done using potential flow for an inviscid fluid but this procedure leaves out certain effects of viscosity which can be included with complete rigor. This kind of analysis using viscous potential flow is carried out here. An exact study of, say air over water requires the inclusion of all of the effects of viscosity, and even the prescription of a basic flow is much more complicated. Problems of superposed viscous fluids have been considered, for example, in the monograph on two-fluid mechanics by Joseph and Renardy [JR] 1991.

Geometry at the interface

The equation of the interface is given by $z-h=0$ (where $h \equiv h(x,y,t)$ is the interface elevation), for which the normal vector $\boldsymbol{N}$ is expressed as

$$\boldsymbol{N} = \nabla\,(z-h) = \left(-\frac{\partial h}{\partial x},\ -\frac{\partial h}{\partial y},\ 1\right), \qquad (2.1)$$

thus the unit normal vector $\boldsymbol{n}$ is expressed as

$$\begin{aligned}\boldsymbol{n} &= \frac{1}{\sqrt{\boldsymbol{N}\cdot\boldsymbol{N}}}\left(-\frac{\partial h}{\partial x},\ -\frac{\partial h}{\partial y},\ 1\right)\\ &= \frac{\left(-\frac{\partial h}{\partial x},\ -\frac{\partial h}{\partial y},\ 1\right)}{\sqrt{1+\left(\frac{\partial h}{\partial x}\right)^2+\left(\frac{\partial h}{\partial y}\right)^2}}.\end{aligned} \qquad (2.2)$$

A unit tangential vector $\boldsymbol{s}$ along the interface may be defined as

$$\boldsymbol{s} = \left(1,\ 0,\ \frac{\partial h}{\partial x}\right)\frac{1}{\ell}, \qquad (2.3)$$

with ℓ defined by

$$\ell = \sqrt{1+\left(\frac{\partial h}{\partial x}\right)^2}. \qquad (2.4)$$

The tangential vector satisfies $\boldsymbol{s}\cdot\boldsymbol{n}=0$. Then the unit binormal vector $\boldsymbol{b}$ may be defined as

$$\begin{aligned}\boldsymbol{b} = \boldsymbol{n}\times\boldsymbol{s} &= \begin{vmatrix} \boldsymbol{e}_1 & \boldsymbol{e}_2 & \boldsymbol{e}_3 \\ n_1 & n_2 & n_3 \\ s_1 & s_2 & s_3 \end{vmatrix}\\ &= \frac{\left(-\frac{1}{\ell}\frac{\partial h}{\partial x}\frac{\partial h}{\partial y},\ \ell,\ \frac{1}{\ell}\frac{\partial h}{\partial y}\right)}{\sqrt{1+\left(\frac{\partial h}{\partial x}\right)^2+\left(\frac{\partial h}{\partial y}\right)^2}}.\end{aligned} \qquad (2.5)$$

These relations can be used to express conditions at the interface.

2.1 Basic equations for Newtonian fluids

We begin by writing the full set of equations for incompressible Newtonian fluids, and then specialize to describe viscous potential flow.

Equations for the air in $0 < z < h_a$ are given by

$$\rho_a\left(\frac{\partial \boldsymbol{v}_a}{\partial t} + U_a\frac{\partial \boldsymbol{v}_a}{\partial x}\right) = -\nabla p_a + \nabla\cdot\tau^{(a)} + \rho_a\boldsymbol{g}, \qquad (2.6)$$

$$\nabla\cdot\boldsymbol{v}_a = 0, \qquad (2.7)$$

$$\bar{p}_a = \text{constant} - \rho_a g z, \qquad (2.8)$$

$$\tau^{(a)} = 2\mu_a e^{(a)} \ \rightarrow\ \tau_{ij}^{(a)} = 2\mu_a e_{ij}^{(a)}, \qquad (2.9a)$$

$$\tau^{(a)} \ \rightarrow\ \tau_{ij}^{(a)} = \tau_{ji}^{(a)}, \qquad (2.9b)$$

$$e^{(a)} \ \rightarrow\ e_{ij} = \frac{1}{2}\left(\frac{\partial v_i}{\partial x_j} + \frac{\partial v_j}{\partial x_i}\right). \qquad (2.9c)$$

The viscous term in (2.6) is to be ignored in viscous potential flow analysis.

Equations for the water in $-h_l < z < 0$ are given by

$$\rho_l\left(\frac{\partial \boldsymbol{v}_l}{\partial t} + U_l\frac{\partial \boldsymbol{v}_l}{\partial x}\right) = -\nabla p_l + \nabla\cdot\tau^{(l)} + \rho_l\boldsymbol{g}, \qquad (2.10)$$

$$\nabla\cdot\boldsymbol{v}_l = 0, \qquad (2.11)$$

$$\bar{p}_l = \text{constant} - \rho_l g z, \qquad (2.12)$$

$$\tau^{(l)} = 2\mu_l e^{(l)} \ \rightarrow\ \tau_{ij}^{(l)} = 2\mu_l e_{ij}^{(l)}, \qquad (2.13a)$$

$$\tau^{(l)} \ \rightarrow\ \tau_{ij}^{(l)} = \tau_{ji}^{(l)}, \qquad (2.13b)$$

$$e^{(l)} \ \rightarrow\ e_{ij} = \frac{1}{2}\left(\frac{\partial v_i}{\partial x_j} + \frac{\partial v_j}{\partial x_i}\right). \qquad (2.13c)$$

The viscous term in (2.10) is to be ignored in viscous potential flow analysis.

Boundary conditions at the interface (at $z = 0 + h \approx 0$, where $h \equiv h(x,y,t)$ is the interface elevation) are given by

$$\frac{\partial h}{\partial t} + U_l\frac{\partial h}{\partial x} = w_l, \quad \frac{\partial h}{\partial t} + U_a\frac{\partial h}{\partial x} = w_a, \ (2.14\text{a, b})$$

$$|\boldsymbol{v}\cdot\boldsymbol{n}|_{dif}=0 \;\rightarrow\; -U_l\frac{\partial h}{\partial x}+w_l=-U_a\frac{\partial h}{\partial x}+w_a, \tag{2.15}$$

$$|\boldsymbol{v}\cdot\boldsymbol{s}|_{dif}=0 \;\rightarrow\; U_l+u_l=U_a+u_a, \tag{2.16}$$

$$|\boldsymbol{v}\cdot\boldsymbol{b}|_{dif}=0 \;\rightarrow\; v_l=v_a, \tag{2.17}$$

$$|s_i\tau_{ij}n_j|_{dif}=0 \;\rightarrow\; \tau_{13}^{(l)}=\tau_{13}^{(a)}, \tag{2.18}$$

$$|b_i\tau_{ij}n_j|_{dif}=0 \;\rightarrow\; \tau_{23}^{(l)}=\tau_{23}^{(a)}, \tag{2.19}$$

$$|n_i\left(-p\delta_{ij}+\tau_{ij}\right)n_j|_{dif}=\gamma\nabla\cdot\boldsymbol{n}$$

$$\rightarrow\; -p_a+\tau_{33}^{(a)}+\rho_a gh-\left(-p_l+\tau_{33}^{(l)}+\rho_l gh\right) =-\gamma\Delta h, \tag{2.20}$$

with the horizontal Laplacian Δ:

$$\Delta=\frac{\partial^2}{\partial x^2}+\frac{\partial^2}{\partial y^2}. \tag{2.21}$$

Equations (2.17) and (2.19) are not needed when we consider two-dimensional disturbances, and (2.16) and (2.18) are not needed for potential flow analysis.

The conditions on the walls are given by

$$w_a=0 \quad \text{at } z=h_a, \tag{2.22a}$$

$$v_a=0 \quad \text{at } y=0,W, \tag{2.22b, c}$$

$$w_l=0 \quad \text{at } z=-h_l, \tag{2.23a}$$

$$v_l=0 \quad \text{at } y=0,W, \tag{2.23b, c}$$

Equations (2.22b,c) and (2.33b,c) cannot be satisfied by potential flow and are dropped in the analysis below.

2.2 Viscous potential flow analysis (2D)

We already noted that if the fluids are allowed to slip at the walls, then the two-dimensional solution will satisfy the three-dimensional equations and we may reduce the analysis to flow between parallel plates. We found that three-dimensional are more stable than two-dimensional disturbances. We now consider 2-dimensional disturbances such as $\boldsymbol{v}=(u,0,w)$, for which the velocity potential $\phi\equiv\phi(x,z,t)$ gives $\boldsymbol{v}=\nabla\phi$, based on the viscous potential theory.

The potential is subject to the equation of continuity:

$$\nabla\cdot\boldsymbol{v}=0 \;\rightarrow\; \frac{\partial u}{\partial x}+\frac{\partial w}{\partial z}=0 \;\rightarrow\; \frac{\partial^2\phi}{\partial x^2}+\frac{\partial^2\phi}{\partial z^2}=0$$

$$\rightarrow\; \Delta\phi+\frac{\partial^2\phi}{\partial z^2}=0 \quad \text{with } \Delta\phi=\frac{\partial^2\phi}{\partial x^2}; \tag{2.24}$$

thus the potentials for the respective fluids are given by

$$\frac{\partial^2\phi_a}{\partial x^2}+\frac{\partial^2\phi_a}{\partial z^2}=0 \quad \text{in } 0<z<h_a, \tag{2.25}$$

$$\frac{\partial^2\phi_l}{\partial x^2}+\frac{\partial^2\phi_l}{\partial z^2}=0 \quad \text{in } -h_l<z<0. \tag{2.26}$$

The potential ϕ_a that satisfies the condition (2.22a) for the air and the potential ϕ_l that satisfies the condition (2.23a) for the water are given, respectively, by

$$\phi_a=A_a\cosh\left[k\left(z-h_a\right)\right]\exp\left(\sigma t+\imath kx\right)+c.c., \tag{2.27a}$$

$$\phi_l=A_l\cosh\left[k\left(z+h_l\right)\right]\exp\left(\sigma t+\imath kx\right)+c.c., \tag{2.27b}$$

and the interface elevation is given by

$$h=A_0\exp\left(\sigma t+\imath kx\right)+c.c., \tag{2.27c}$$

where A_a, A_l and A_0 denote the complex amplitude, and $c.c.$ stands for the complex conjugate of the preceding expression; σ is the complex growth rate and k denotes the wavenumber; $\imath=\sqrt{-1}$. From the kinematic conditions (2.14a,b), we have the following equations for the complex amplitudes:

$$\left(\sigma+\imath kU_a\right)A_0=-kA_a\sinh\left(kh_a\right), \tag{2.28a}$$

$$\left(\sigma+\imath kU_l\right)A_0=kA_l\sinh\left(kh_l\right). \tag{2.28b}$$

The other boundary condition is the normal stress balance (with the normal viscous stress) at the interface, (2.20):

$$-p_a+\tau_{33}^{(a)}+\rho_a gh-\left(-p_l+\tau_{33}^{(l)}+\rho_l gh\right)=-\gamma\Delta h, \tag{2.29}$$

in which the pressure p_a included may be written, from the equation of motion without the viscous term, as

$$\rho_a \left(\frac{\partial u_a}{\partial t} + U_a \frac{\partial u_a}{\partial x} \right) = -\frac{\partial p_a}{\partial x},$$

and with the aid of the equation of continuity, we have the expression of p_a

$$\rho_a \left(\frac{\partial^2 w_a}{\partial t \partial z} + U_a \frac{\partial^2 w_a}{\partial x \partial z} \right) = \frac{\partial^2 p_a}{\partial x^2}; \qquad (2.30a)$$

the pressure p_l may be written as

$$\rho_l \left(\frac{\partial^2 w_l}{\partial t \partial z} + U_l \frac{\partial^2 w_l}{\partial x \partial z} \right) = \frac{\partial^2 p_l}{\partial x^2}. \qquad (2.30b)$$

Thus the normal stress balance is now written as

$$-\rho_a \left(\frac{\partial^2 w_a}{\partial t \partial z} + U_a \frac{\partial^2 w_a}{\partial x \partial z} \right) + 2\mu_a \Delta \frac{\partial w_a}{\partial z} + \rho_a g \Delta h$$
$$+ \rho_l \left(\frac{\partial^2 w_l}{\partial t \partial z} + U_l \frac{\partial^2 w_l}{\partial x \partial z} \right) - 2\mu_l \Delta \frac{\partial w_l}{\partial z} - \rho_l g \Delta h$$
$$= -\gamma \Delta^2 h, \qquad (2.31)$$

which is then written as

$$\left[-\rho_a k^2 (\sigma + \imath k U_a) - 2\mu_a k^4 \right] A_a \cosh(k h_a)$$
$$+ \left[\rho_l k^2 (\sigma + \imath k U_l) + 2\mu_l k^4 \right] A_l \cosh(k h_l)$$
$$-\rho_a g k^2 A_0 + \rho_l g k^2 A_0 = -\gamma k^4 A_0,$$

so that we have the equation of σ, using (2.27) and (2.28) and assuming $A_0 \neq 0$:

$$\left[\rho_a (\sigma + \imath k U_a)^2 + 2\mu_a k^2 (\sigma + \imath k U_a) \right] \coth(k h_a)$$
$$+ \left[\rho_l (\sigma + \imath k U_l)^2 + 2\mu_l k^2 (\sigma + \imath k U_l) \right] \coth(k h_l)$$
$$+ (\rho_l - \rho_a) g k + \gamma k^3 = 0.$$

2.3 Dispersion relation

Thus the dispersion relation is given as

$$[\rho_a \coth(k h_a) + \rho_l \coth(k h_l)] \sigma^2$$
$$+2\sigma \left\{ \imath k [\rho_a U_a \coth(k h_a) + \rho_l U_l \coth(k h_l)] + k^2 [\mu_a \coth(k h_a) + \mu_l \coth(k h_l)] \right\}$$
$$-k^2 \left[\rho_a U_a^2 \coth(k h_a) + \rho_l U_l^2 \coth(k h_l) \right] + 2\imath k^3 [\mu_a U_a \coth(k h_a) + \mu_l U_l \coth(k h_l)]$$
$$+ (\rho_l - \rho_a) g k + \gamma k^3 = 0. \qquad (2.32)$$

If the top and bottom are far away $h_l \to \infty, h_a \to \infty$, then (2.32) reduces to the problem considered by [JLF]:

$$\sigma = -\frac{\imath k (\rho_a U_a + \rho_l U_l) + k^2 (\mu_a + \mu_l)}{(\rho_a + \rho_l)}$$
$$\pm \left[\frac{\rho_a \rho_l k^2 (U_a - U_l)^2}{(\rho_a + \rho_l)^2} - \frac{(\rho_l - \rho_a) g k + \gamma k^3}{(\rho_a + \rho_l)} + \frac{k^4 (\mu_a + \mu_l)^2}{(\rho_a + \rho_l)^2} + 2\imath k^3 \frac{(\rho_a \mu_l - \rho_l \mu_a)(U_a - U_l)}{(\rho_a + \rho_l)^2} \right]^{1/2},$$

which is reduced, for a particular case that $\rho_a \mu_l = \rho_l \mu_a$, to

$$\sigma_R = -\frac{k^2 (\mu_a + \mu_l)}{(\rho_a + \rho_l)} \pm \left[\frac{\rho_a \rho_l k^2 (U_a - U_l)^2}{(\rho_a + \rho_l)^2} - \frac{(\rho_l - \rho_a) g k + \gamma k^3}{(\rho_a + \rho_l)} + \frac{k^4 (\mu_a + \mu_l)^2}{(\rho_a + \rho_l)^2} \right]^{1/2},$$
$$\sigma_I = -\frac{k (\rho_a U_a + \rho_l U_l)}{(\rho_a + \rho_l)}.$$

Here, it is easy to find that the equation $\sigma_R = 0$ gives a relation being irrespective of viscosity. In other words, the relation holds even for inviscid fluids; this is much suggestive for the problem to be considered herein.

To facilitate further analysis we may write (2.32) as

$$A\sigma^2 + 2B\sigma + C = 0, \tag{2.33}$$

where the coefficients A, B and C are defined as

$$A = \rho_l \coth(kh_l) + \rho_a \coth(kh_a), \tag{2.34a}$$

$$B = \imath k\left[\rho_l U_l \coth(kh_l) + \rho_a U_a \coth(kh_a)\right] + k^2\left[\mu_l \coth(kh_l) + \mu_a \coth(kh_a)\right] = B_R + \imath B_I, \tag{2.34b}$$

$$\begin{aligned} C = (\rho_l - \rho_a) gk - k^2\left[\rho_l U_l^2 \coth(kh_l) + \rho_a U_a^2 \coth(kh_a)\right] + \gamma k^3 \\ +2\imath k^3\left[\mu_l U_l \coth(kh_l) + \mu_a U_a \coth(kh_a)\right] = C_R + \imath C_I. \end{aligned} \tag{2.34c}$$

The solution σ may be expressed as

$$\sigma = -\frac{B}{A} \pm \sqrt{\frac{B^2}{A^2} - \frac{C}{A}} \quad \rightarrow \quad \sigma_R + \imath\sigma_I = -\frac{B_R + \imath B_I}{A} \pm \sqrt{\left(\frac{B_R + \imath B_I}{A}\right)^2 - \frac{C_R + \imath C_I}{A}}, \tag{2.35}$$

$$\sigma = -\frac{B}{A} \pm \frac{\sqrt{D}}{A} \quad \rightarrow \quad \sigma_R + \imath\sigma_I = -\frac{B_R + \imath B_I}{A} \pm \frac{\sqrt{D}}{A}$$

where D is given by

$$\begin{aligned} D = D_R + \imath D_I = (B_R + \imath B_I)^2 - A(C_R + \imath C_I), \\ D_R = \rho_l \rho_a (U_a - U_l)^2 k^2 \coth(kh_l)\coth(kh_a) + k^4\left[\mu_l \coth(kh_l) + \mu_a \coth(kh_a)\right]^2 \\ -\left[\rho_l \coth(kh_l) + \rho_a \coth(kh_a)\right]\left[(\rho_l - \rho_a) gk + \gamma k^3\right], \\ D_I = 2k^3 (\rho_a \mu_l - \rho_l \mu_a)(U_a - U_l)\coth(kh_l)\coth(kh_a). \end{aligned}$$

When $\rho_a \mu_l = \rho_l \mu_a$ for which $D_I = 0$, and if $D_R \geq 0$, we have

$$\sigma_R = \frac{-B_R \pm \sqrt{D_R}}{A}, \quad \sigma_I = -\frac{B_I}{A}.$$

This is a typical case where the real and imaginary parts of σ can be expressed most clearly.

2.4 Growth rates and wave speeds

In terms of $\sigma = \sigma_R + \imath\sigma_I$, (2.33) is also written as

$$A(\sigma_R + \imath\sigma_I)^2 + 2(B_R + \imath B_I)(\sigma_R + \imath\sigma_I) + (C_R + \imath C_I) = 0,$$

for which the real and imaginary parts are given as

$$A\left(\sigma_R^2 - \sigma_I^2\right) + 2(B_R\sigma_R - B_I\sigma_I) + C_R = 0, \tag{2.36a}$$

$$2A\sigma_R\sigma_I + 2B_R\sigma_I + 2B_I\sigma_R + C_I = 0 \quad \rightarrow \quad \sigma_I = -\frac{2B_I\sigma_R + C_I}{2(A\sigma_R + B_R)} = -\frac{B_I\sigma_R + \frac{C_I}{2}}{A\sigma_R + B_R}. \tag{2.36b}$$

Eliminating σ_I from the above, we have a quartic equation for σ_R:

$$A\left[\sigma_R^2\left(A\sigma_R+B_R\right)^2-\left(B_I\sigma_R+\frac{C_I}{2}\right)^2\right]+2B_R\sigma_R\left(A\sigma_R+B_R\right)^2$$

$$+2B_I\left(B_I\sigma_R+\frac{C_I}{2}\right)\left(A\sigma_R+B_R\right)+C_R\left(A\sigma_R+B_R\right)^2=0,$$

which is then written as

$$a_4\sigma_R^4+a_3\sigma_R^3+a_2\sigma_R^2+a_1\sigma_R+a_0=0, \tag{2.37}$$

where the coefficients are given as

$$a_4=A^3, \tag{2.38a}$$

$$a_3=2A^2B_R+2A^2B_R=4A^2B_R, \tag{2.38b}$$

$$a_2=AB_R^2-AB_I^2+4AB_R^2+2AB_I^2+A^2C_R=5AB_R^2+AB_I^2+A^2C_R, \tag{2.38c}$$

$$a_1=-AB_IC_I+2B_R^3+AB_IC_I+2B_RB_I^2+2AB_RC_R=2B_R^3+2B_RB_I^2+2AB_RC_R, \tag{2.38d}$$

$$a_0=-\frac{1}{4}AC_I^2+B_RB_IC_I+B_R^2C_R. \tag{2.38e}$$

The quartic equation (2.37) can be solved analytically. Neutral states for which $\sigma_R=0$ are described in terms of the solution to the equation $a_0=0$. The peak value *(the maximum growth rate)* σ_m and the corresponding wavenumber k_m are obtained by solving (2.37). It is usually true, but unproven, that $\lambda_m=2\pi/k_m$ will be the length of unstable waves observed in experiments.

The complex values of σ are frequently expressed in terms of a complex frequency ω with

$$\sigma_R+\imath\sigma_I=\sigma=-\imath\omega=-\imath\omega_R+\omega_I.$$

Hence

$$\sigma_R=\omega_I;\quad \sigma_I=-\omega_R.$$

The wave speed for the mode with wavenumber k is

$$\tilde{C}_R=\omega_R/k=-\sigma_I/k.$$

The set of wavenumbers for which unstable flows are stable is also of interest. The wavelengths corresponding to these wavenumbers will not appear in the spectrum. *Cut-off wavenumbers* k_C separate the unstable and stable parts of the specturm.

2.5 Neutral curves

Neutral curves define values of the parameters for which $\sigma_R(k)=0$. These curves may be obtained by putting $a_0=0$

$$-\frac{\rho_l\mu_a^2\coth\left(kh_l\right)\coth^2\left(kh_a\right)+\rho_a\mu_l^2\coth^2\left(kh_l\right)\coth\left(kh_a\right)}{\left[\mu_l\coth\left(kh_l\right)+\mu_a\coth\left(kh_a\right)\right]^2}kV^2+\left(\rho_l-\rho_a\right)g+\gamma k^2=0, \tag{2.39}$$

where the relative velocity V is defined by $V\equiv U_a-U_l$. This equation may be solved for V^2 where

$$V^2(k)=\frac{\left[\mu_l\coth\left(kh_l\right)+\mu_a\coth\left(kh_a\right)\right]^2}{\rho_l\mu_a^2\coth\left(kh_l\right)\coth^2\left(kh_a\right)+\rho_a\mu_l^2\coth^2\left(kh_l\right)\coth\left(kh_a\right)}\frac{1}{k}\left[\left(\rho_l-\rho_a\right)g+\gamma k^2\right]. \tag{2.40}$$

The lowest point on the neutral curve $V^2(k)$ is

$$V_c^2 = \min_{k \geq 0} V^2(k) \equiv V^2(k_c)$$

where $\lambda_c = 2\pi/k_c$ is the wave length that makes V^2 minimum. The flow is unstable when

$$V^2 = (-V)^2 > V_c^2.$$

This criteria is symmetric with respect to V and $-V$, depending only on the absolute value of the relative velocity. This feature stems from Galilean invariance; the flow seen by the observer moving with gas is the same as the one seen by an observer moving with the liquid.

3 K-H Instability of Inviscid Fluid

For inviscid fluids, we have $B_R = 0$ and $C_I = 0$; thus $a_3 = a_1 = a_0 = 0$ and (2.37) reduces to

$$a_4\sigma_R^4 + a_2\sigma_R^2 = 0, \tag{3.1}$$

Thus, we have

$$a_4\sigma_R^2 + a_2 = 0 \;\rightarrow\; A^3\sigma_R^2 + AB_I^2 + A^2C_R = 0, \tag{3.2}$$

and

$$\sigma_I = -\frac{B_I\sigma_R + \dfrac{C_I}{2}}{A\sigma_R + B_R} = -\frac{B_I}{A} = -\frac{k\left[\rho_l U_l \coth(kh_l) + \rho_a U_a \coth(kh_a)\right]}{\rho_l \coth(kh_l) + \rho_a \coth(kh_a)}. \tag{3.3}$$

It should be noted here that the neutral curve was given by the equation $a_0 = 0$ in the viscous potential analysis ((2.39) and (2.40)), whereas the neutral curve in this K-H instability is given by the equation $a_2 = 0$.

From (3.2) with $a_2 < 0$, the growth rate σ_R is expressed as

$$\sigma_R = \pm\sqrt{-\frac{B_I^2}{A^2} - \frac{C_R}{A}}$$

$$= \pm\frac{\sqrt{\rho_l\rho_a k^2 \coth(kh_l)\coth(kh_a)\,V^2 - \left[\rho_l \coth(kh_l) + \rho_a \coth(kh_a)\right]\left[(\rho_l - \rho_a)\,gk + \gamma k^3\right]}}{\rho_l \coth(kh_l) + \rho_a \coth(kh_a)}. \tag{3.4}$$

At the neutral state $\sigma_R = 0$ for which $a_2 = 0$, we have

$$\frac{\rho_l\rho_a k \coth(kh_l)\coth(kh_a)}{\rho_l \coth(kh_l) + \rho_a \coth(kh_a)}V^2 - \left[(\rho_l - \rho_a)\,g + \gamma k^2\right] = 0. \tag{3.5}$$

Instability arises if

$$V^2 > \left[\frac{\tanh(kh_l)}{\rho_l} + \frac{\tanh(kh_a)}{\rho_a}\right]\frac{1}{k}\left[(\rho_l - \rho_a)\,g + \gamma k^2\right] \equiv V_i^2(k). \tag{3.6}$$

In the stable case for which $a_2 > 0$, the wave velocity $\tilde{C}_R$ is given by

$$-k\tilde{C}_R = \sigma_I = -\frac{B_I}{A} \pm \sqrt{\frac{B_I^2}{A^2} + \frac{C_R}{A}}. \tag{3.7}$$

4 Dimensionless form of the dispersion equation

The dimensionless variables are designated with a roof and are listed below

$$\begin{aligned}
\hat{k} &= kH, & \hat{U}_a &= \frac{U_a}{Q},\\
\hat{h}_a &= \frac{h_a}{H} \equiv \alpha, & \hat{U}_l &= \frac{U_l}{Q},\\
\hat{h}_l &= \frac{h_l}{H} = 1 - \hat{h}_a, & \hat{V} &= \hat{U}_a - \hat{U}_l\\
\hat{\rho} &= \frac{\rho_a}{\rho_l}, & \hat{\sigma} &= \frac{\sigma H}{Q},\\
\hat{\mu} &= \frac{\mu_a}{\mu_l}, & \theta &= \frac{\mu_l}{\rho_l H Q},\\
\hat{\gamma} &= \frac{\gamma}{\rho_l g H^2}, &&
\end{aligned}$$

where

$$Q = \left[\frac{(1-\hat{\rho})gH}{\hat{\rho}}\right]^{1/2}.$$

The dimensionless form of (2.32) is given by

$$\begin{aligned}
\Big[\coth(\hat{k}\hat{h}_l) &+ \hat{\rho}\coth(\hat{k}\hat{h}_a)\Big]\,\hat{\sigma}^2\\
&+ 2\hat{\sigma}\left\{i\hat{k}\left[\hat{U}_l\coth(\hat{k}\hat{h}_l) + \hat{\rho}\hat{U}_a\coth(\hat{k}\hat{h}_a)\right] + \theta\hat{k}^2\left[\coth(\hat{k}\hat{h}_l) + \hat{\mu}\coth(\hat{k}\hat{h}_a)\right]\right\}\\
&- \hat{k}^2\left[\hat{U}_l^2\coth(\hat{k}\hat{h}_l) + \hat{\rho}\hat{U}_a^2\coth(\hat{k}\hat{h}_a)\right] + 2i\hat{k}^3\theta\left[\hat{U}_l\coth(\hat{k}\hat{h}_l) + \hat{\mu}\hat{U}_a\coth(\hat{k}\hat{h}_a)\right]\\
&+ \hat{k}\left[1 + \frac{\hat{\gamma}\hat{k}^2}{(1-\hat{\rho})}\right] = 0. \qquad (4.1)
\end{aligned}$$

The expression (2.40) for the neutral curve $\hat{\sigma}_R(\hat{k}) = 0$ is written in dimensionless variables as

$$\hat{V}^2 = \frac{\Big[\tanh(\hat{k}\hat{h}_a) + \hat{\mu}\tanh(\hat{k}\hat{h}_l)\Big]^2}{\tanh(\hat{k}\hat{h}_a) + (\hat{\mu}^2/\hat{\rho})\tanh(\hat{k}\hat{h}_l)}\,\frac{1}{\hat{k}}\left[1 + \frac{\hat{\gamma}\hat{k}^2}{(1-\hat{\rho})}\right]. \qquad (4.2)$$

Notice that the growth rate parameter $\theta = \mu_l/(\rho_l Q)$, which depends linearly on the kinematic viscosity $\nu_l = \mu_l/\rho_l$ of the liquid does not appear in (4.2).

The neutral curves for an inviscid fluid (3.5) can be obtained by putting $\hat{\mu} = \hat{\rho}$ or $\mu_l/\rho_l = \mu_a/\rho_a$. This gives

$$\begin{aligned}
\hat{V}^2 &= \frac{\Big[\tanh(\hat{k}\hat{h}_a) + \hat{\rho}\tanh(\hat{k}\hat{h}_l)\Big]^2}{\Big[\tanh(\hat{k}\hat{h}_a) + \hat{\rho}\tanh(\hat{k}\hat{h}_l)\Big]}\,\frac{1}{\hat{k}}\left[1 + \frac{\hat{\gamma}\hat{k}^2}{1-\hat{\rho}}\right]\\
&= \Big[\tanh(\hat{k}\hat{h}_a) + \hat{\rho}\tanh(\hat{k}\hat{h}_l)\Big]\,\frac{1}{\hat{k}}\left[1 + \frac{\hat{\gamma}\hat{k}^2}{1-\hat{\rho}}\right] \qquad (4.3)
\end{aligned}$$

which is the dimensionless form of (3.6). Though this reduction is immediate it is surprising.

Evaluating (4.2) for $\hat{\mu} = 0$, we get

$$\hat{V}^2 = \tanh(\hat{k}\hat{h}_a)\frac{1}{\hat{k}}\left[1 + \frac{\hat{\gamma}\hat{k}^2}{1-\hat{\rho}}\right]. \tag{4.4}$$

Evaluating (4.2) for $\hat{\mu} = \infty$ we get

$$\hat{V}^2 = \hat{\rho}\tanh(\hat{k}h_l)\,\frac{1}{\hat{k}}\left[1 + \frac{\hat{\gamma}\hat{k}^2}{1-\hat{\rho}}\right]. \tag{4.5}$$

It is easy to verify that $\hat{V}^2$ is maximum at $\hat{\mu} = \hat{\rho}$, for inviscid fluids. Viscosity in viscous potential flow is destablizing; however, large viscosities are less destabilizing than small viscosities.

Since $\hat{\rho} = 0.0012$, it is very small, the variation in the stability is large as $\hat{\mu}$ varies between $\hat{\rho}$ and ∞, and is very small as $\hat{\mu}$ varies between $\hat{\rho}$ and zero. The value $\hat{\mu} = 0.018 > \hat{\rho} = 0.0012$, and is in the interval in which $\hat{V}^2$ is rapidly varying (see figure 4).

In the literature on gas liquid flows a long wave approximation is often made to obtain stability limits. For long waves $\hat{k} \to 0$ and $\tanh(\hat{k}\hat{h}) \to \hat{k}\hat{h}$ and (4.2) reduces to

$$\hat{V}^2 = \frac{(\hat{h}_a + \hat{\mu}\hat{h}_l)^2}{\left[\hat{h}_a + (\hat{\mu}^2/\hat{\rho})\hat{h}_l\right]}\left[1 + \frac{\hat{\gamma}\hat{k}^2}{1-\hat{\rho}}\right]. \tag{4.6}$$

The effect of surface tension disappears in this limit but the effects of viscosity are important. To get the long wave limit in the inviscid case put $\hat{\mu} = \hat{\rho}$.

The regularization of short waves by surface tension is an important physical effect. For short waves, $\hat{k} \to \infty$, $\tanh(\hat{k}\hat{h}) \to 1$ and

$$\hat{V}^2 = \frac{(\hat{\mu}+1)^2}{1+\hat{\mu}^2/\hat{\rho}}\frac{1}{\hat{k}}\left[1 + \frac{\hat{\gamma}\hat{k}^2}{(1-\hat{\rho})}\right]. \tag{4.7}$$

To get the short wave limit in the inviscid case put $\hat{\mu} = \hat{\rho}$.

The effects of surface tension may be computed from (4.6) and (4.7). The stability limit for long waves $\hat{k} \to 0$ is independent of $\hat{\gamma}$. For short waves (4.6) has a minimum at $\hat{k} = \sqrt{(1-\hat{\rho})/\hat{\gamma}}$ with a value there given by

$$\hat{V}^2 = \frac{2(\hat{\mu}+1)^2}{1+\hat{\mu}^2/\hat{\rho}}\sqrt{\frac{1-\hat{\rho}}{\hat{\gamma}}}. \tag{4.8}$$

Equation (4.8) shows that short waves are stablized by increasing $\hat{\gamma}$. For small $\hat{\gamma}$ instability is for long waves.

5 The effect of liquid viscosity and surface tension on growth rates and neutral curves

For air and water at 20°C

$$\rho_a = 0.0012\,\mathrm{g/cm^3}, \qquad \rho_l = 1\,\mathrm{g/cm^3}, \quad \hat{\rho} = \rho_a/\rho_l = 0.0012,$$

$$\mu_a = 0.00018\,\text{poise}, \quad \mu_l = 0.01\,\text{poise}, \quad \hat{\mu} = \mu_a/\mu_l = 0.018.$$

The surface tension of air and pure water is $\gamma = 72.8$dynes/cm. Usually the water is slightly contaminated and $\gamma = 60$dynes/cm is more probable for the water-air tension in experiments. For all kinds of organic liquids a number like $\gamma = 30$dynes/cm is close to the mark.

Neutral curves for $\hat{\mu} = 0.018$ (air/water) and $\hat{\mu} = \hat{\rho} = 0.0012$ (inviscid flow) and $\hat{\mu} = 3.6 \times 10^{-6}$ ($\mu_l = 50$ poise) with $\gamma = 60$dynes/cm are shown in figures 1, 2 and 3. The liquid viscosities $\mu_l = \rho_l \mu_a/\rho_a$ corresponding to these three cases are $\mu_l = 0.01$ poise, 0.15 poise and 50 poise. The neutral curves for $\hat{\mu} \geq \hat{\rho}$ are nearly identical. The neutral curves for $\hat{\mu} = 0.018$ (air/water) are to be compared with experiments. We have indentified the minimum values of (4.2) over $\hat{k} \geq 0$ in the air/water case, and in tables 1, 2 and 3 the critical velocity $V_c = V(k_c)$, the critical wave number k_c (and wave length $\lambda_c = 2\pi/k_c$) and associated wave speeds $\tilde{C}_{Rc} = \tilde{C}_R(k_c)$ are listed. In the tables, V_s and $\tilde{C}_{Rs}$ denote the values taken at $k = 10^{-3}$[1/cm], which may be representative of values in the limit of long wave, $k \to 0$. The variation of the critical velocity with the viscosity ratio $\hat{\mu} = \mu_a/\mu_l$ for a representative gas fraction $\alpha = 0.5$ is shown in figure 4. The vertical line $\hat{\mu} = \hat{\rho}$ identifies the stability limit for inviscid fluids. Points to the left of this line have high liquid viscosities $\mu_l > 0.15$ poise, and for points to the right, $\mu_l < 0.15$ poise.

In all cases the critical velocity is influenced by surface tension; the critical velocity is given by long waves only when α is small (small air gaps). For larger values of α (say $\alpha > 0.2$), the most dangerous neutrally unstable wave is identified by a sharp minimum determined by surface tension, which is identified in table 1 (*c.f.* equation (4.8)).

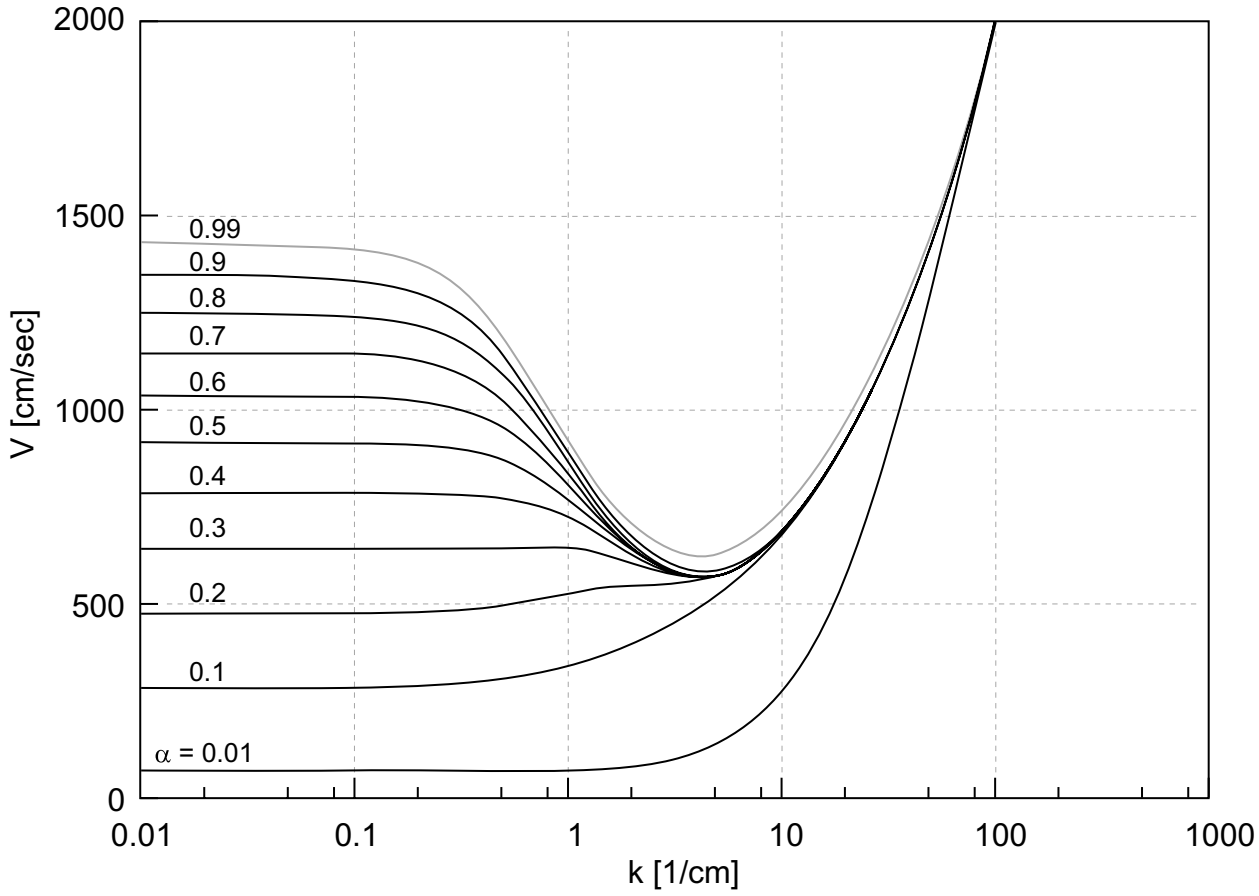

Figure 1: *Neutral curves for air and water ($\hat{\mu} = 0.018$, see table 1); $\alpha = \hat{h}_a$ is the gas fraction.*

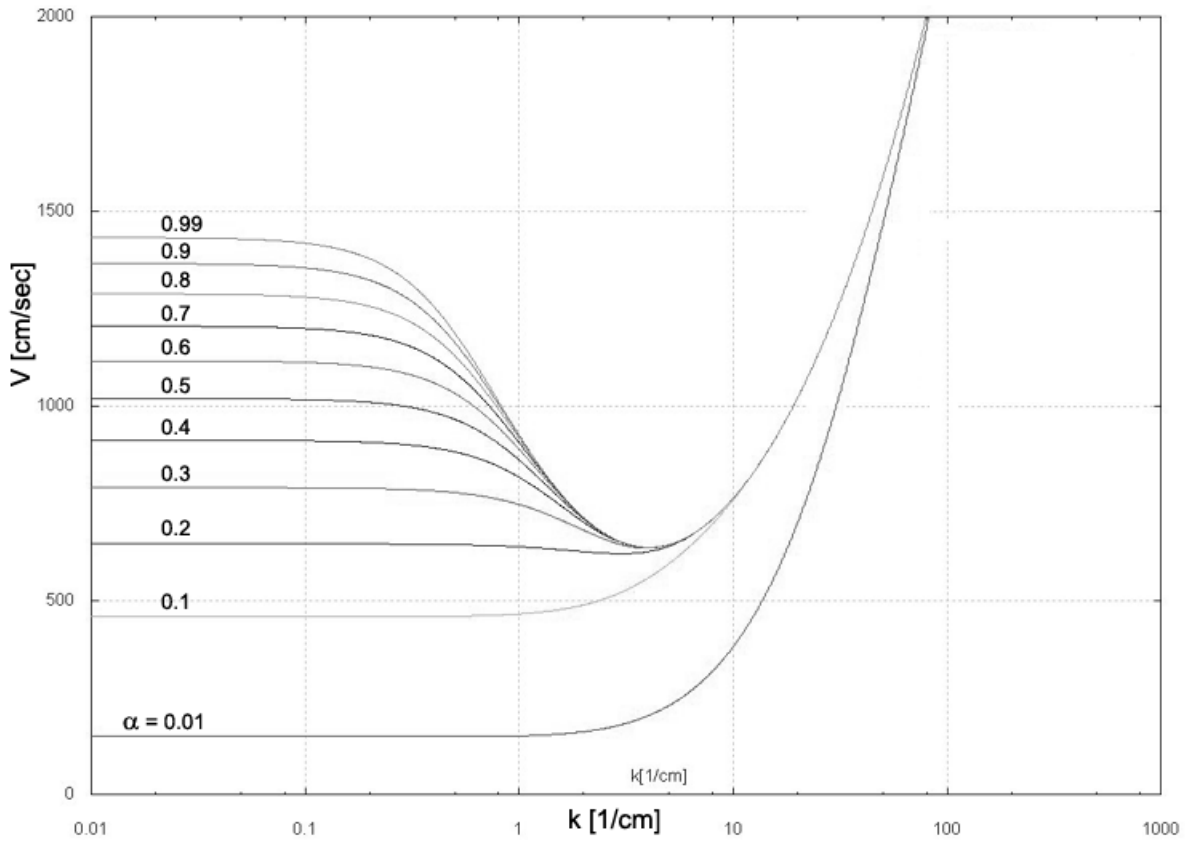

Figure 2: *Neutral curves for inviscid fluids ($\hat{\mu} = \hat{\rho} = 0.0012$) for different gas fractions $\alpha = \hat{h}_a$. This neutral curve arose for the special case $\hat{\mu} = \hat{\rho} = 0.0012 = \mu_a/\mu_l$ with $\mu_a = 0.00018$ poise; hence $\mu_l = 0.15$ poise. Surprisingly it is identical to the case $\mu_a = \mu_l = 0$ (see table 2).*

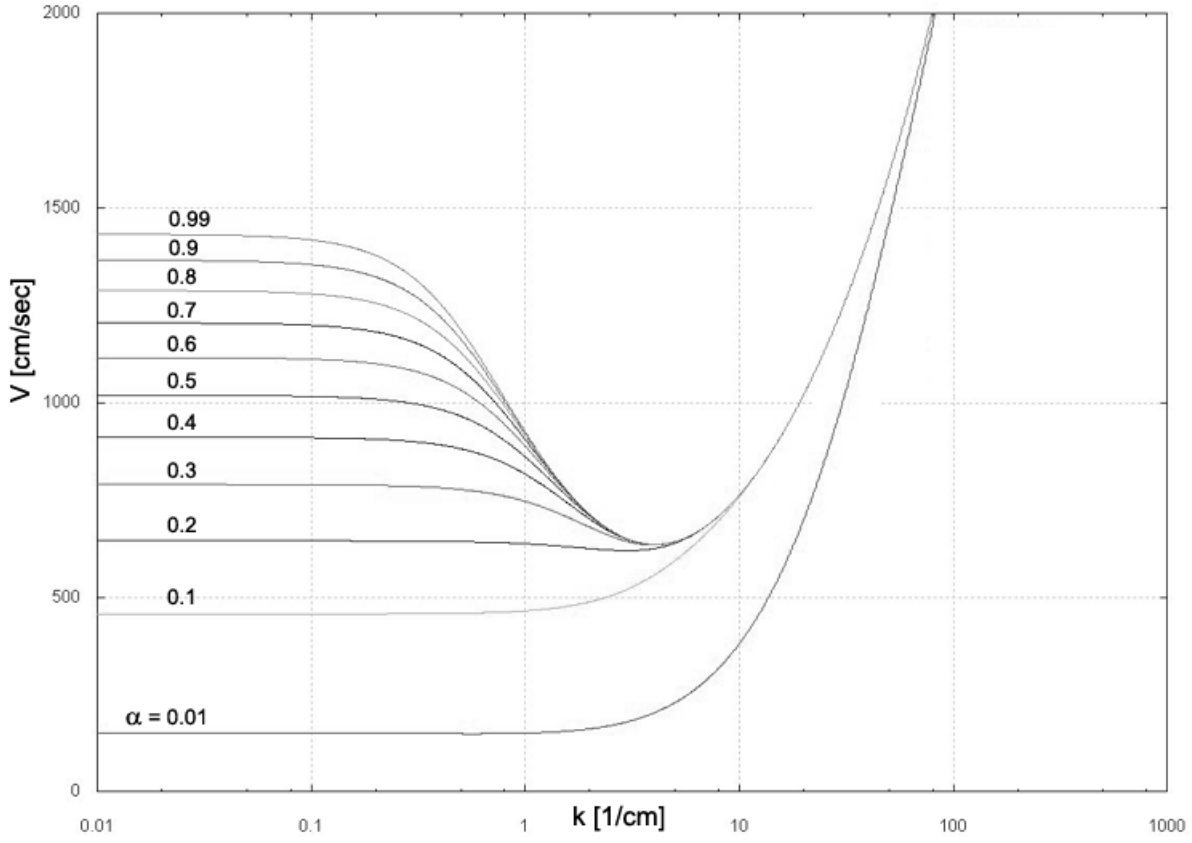

Figure 3: *Neutral curves for liquid air and* $\mu_l = 50$ *poise liquid* ($\hat{\mu} = 3.6 \times 10^{-6}$) *for different gas fractions* $\alpha = \hat{h}_a$ *(see table 3). The neutral curves for viscous liquid with* $\mu_l > 0.15$ *poise are essentially identical to the neutral curves for inviscid liquid.*

Table 1: ρ_a =*0.0012[g/cm^3]*, μ_a =*0.00018[g/cm/sec]*, ρ_l =*1.0[g/cm^3]*, μ_l =*0.01[g/cm/sec]*, g =*980.0[cm/sec^2]*, γ =*60.0[dynes/cm]*, H =*2.54[cm]*.

$\hat{h}_a$	V_s[cm/sec]	$\tilde{C}_{Rs}$[cm/sec]	k_c[1/cm]	λ_c[cm]	V_c[cm/sec]	$\tilde{C}_{Rc}$[cm/sec]
0.01	76.0432	198.5692	0.6494	9.6756	72.9167	155.8590
0.1	285.5866	43.2185				
0.2	478.4722	20.8209				
0.3	643.4475	12.4952	0.6923	9.0762	651.2637	9.4315
			3.8929	1.6140	572.5005	5.5099
0.4	788.7526	8.1499	4.0195	1.5632	573.9078	5.4843
0.5	919.4103	5.4813	4.0517	1.5507	574.0776	5.4813
0.6	1038.7081	3.6759	4.0517	1.5507	574.1212	5.4785
0.7	1148.9159	2.3731	4.0517	1.5507	574.3082	5.4590
0.8	1251.6682	1.3888	4.1170	1.5261	575.6849	5.3194
0.9	1348.1820	0.6188	4.3540	1.4431	585.3108	4.4148
0.99	1430.4848	0.0564	4.1501	1.5140	628.0101	0.5849

Table 2: ρ_a =*0.0012[g/cm^3]*, μ_a =*0.0[g/cm/sec]*, ρ_l =*1.0[g/cm^3]*, μ_l =*0.0[g/cm/sec]*, g =*980.0[cm/sec^2]*, γ =*60.0[dynes/cm]*, H =*2.54[cm]*.

$\hat{h}_a$	V_s[cm/sec]	$\tilde{C}_{Rs}$[cm/sec]	k_c[1/cm]	λ_c[cm]	V_c[cm/sec]	$\tilde{C}_{Rc}$[cm/sec]
0.01	152.2491	16.1666	0.6289	9.9901	150.6110	9.7248
0.1	457.6265	4.8896				
0.2	645.2579	3.0824	2.9902	2.1013	619.8183	0.8176
0.3	789.4894	2.2044	3.9242	1.6011	634.4431	0.7643
0.4	911.1691	1.6372	4.0195	1.5632	635.7381	0.7624
0.5	1018.4128	1.2206	4.0517	1.5507	635.8945	0.7622
0.6	1115.3923	0.8916	4.0517	1.5507	635.9132	0.7618
0.7	1204.5893	0.6192	4.0517	1.5507	635.9142	0.7590
0.8	1287.6220	0.3862	4.0517	1.5507	635.9038	0.7377
0.9	1365.6153	0.1821	4.0517	1.5507	635.8298	0.5897
0.99	1432.1824	0.0174	4.0517	1.5507	635.5740	0.0782

Table 3: ρ_a =*0.0012[g/cm^3]*, μ_a =*0.00018[g/cm/sec]*, ρ_l =*1.0[g/cm^3]*, μ_l =*50.0[g/cm/sec]*, g =*980.0[cm/sec^2]*, γ =*60.0[dynes/cm]*, H =*2.54[cm]*.

$\hat{h}_a$	V_s[cm/sec]	$\tilde{C}_{Rs}$[cm/sec]	k_c[1/cm]	λ_c[cm]	V_c[cm/sec]	$\tilde{C}_{Rc}$[cm/sec]
0.01	143.9903	0.1104				
0.1	455.1899	0.0100				
0.2	643.7241	0.0045	1.9889	3.1591	637.6000	0.0015
0.3	788.3930	0.0026	3.4807	1.8051	664.1580	0.0011
0.4	910.3551	0.0017	3.6227	1.7344	666.6147	0.0011
0.5	1017.8060	0.0011	3.6517	1.7206	666.9543	0.0011
0.6	1114.9491	0.0007	3.6517	1.7206	667.0070	0.0011
0.7	1204.2815	0.0005	3.6811	1.7069	667.0151	0.0011
0.8	1287.4300	0.0003	3.6811	1.7069	667.0162	0.0011
0.9	1365.5248	0.0001	3.6811	1.7069	667.0158	0.0008
0.99	1432.1738	1.1 $\times 10^{-5}$	3.6811	1.7069	667.0143	0.0001

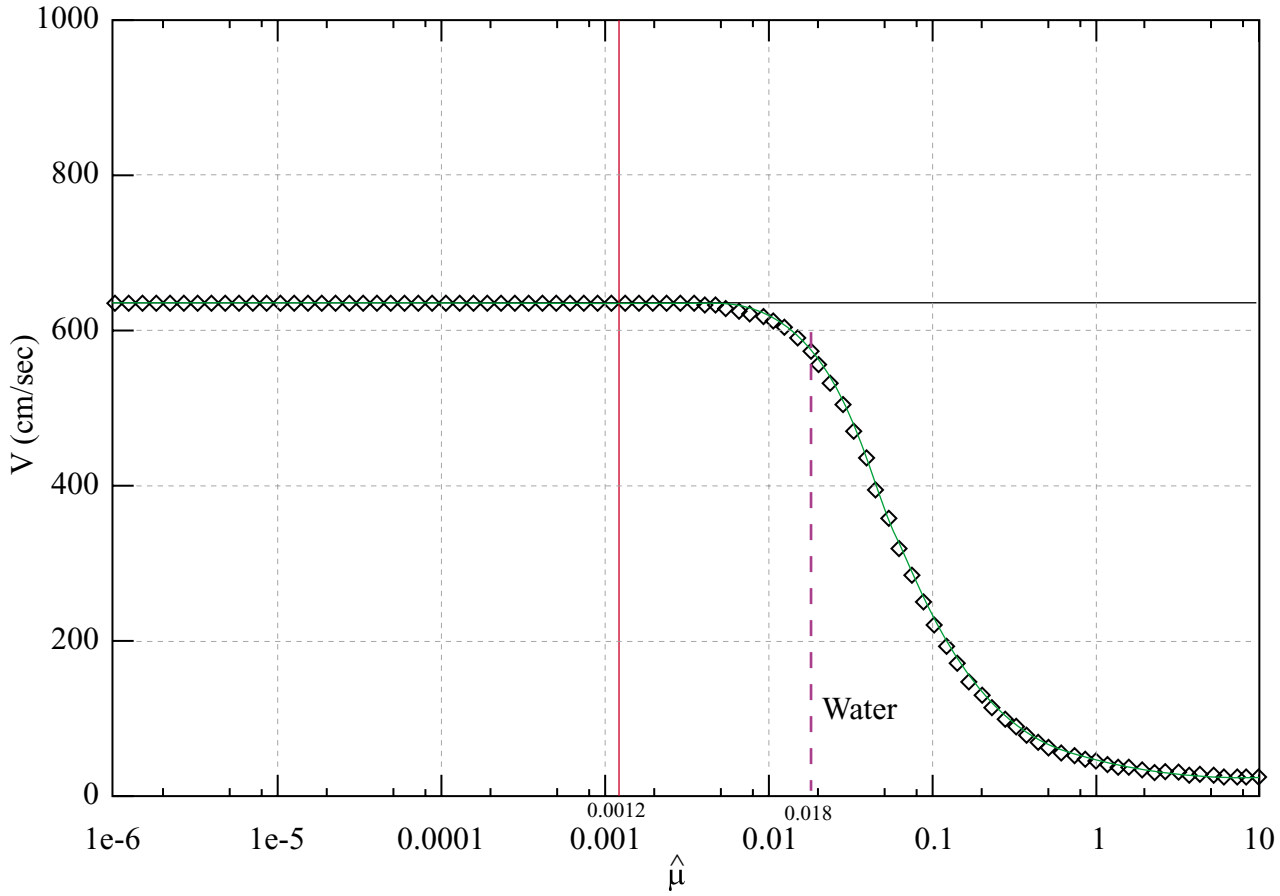

Figure 4: *Critical velocity V vs. $\hat{\mu}$ for $\alpha = 0.5$. The critical velocity is the minimum value on the neutral curve. The vertical line is $\hat{\mu} = \hat{\rho} = 0.0012$ and the horizontal line at $V = 635.9 cm/sec$ is the critical value for inviscid fluids. The vertical dashed line at $\hat{\mu} = 0.018$ is for air and water.*

Growth rates for the same three cases as in figures 1, 2, and 3, are shown in figures 5a-c, 6a-c, and 7a-c. The growth rates depend strongly on the liquid viscosity unlike the neutral curves. The most dangerous linear wave is the one whose growth rate σ_R is maximum at $k = k_m$,

$$\sigma_{Rm} = \sigma_R(k_m) = \max_{k \geq 0} \sigma_R(k) \tag{5.1}$$

with an associated wavelength $\lambda_m = 2\pi/k_m$ and wave speed $\tilde{C}_{Rm} = \tilde{C}_R(k_m)$. The values of these parameters for the most unstable waves are listed in the captions to figures 5, 6 and 7.

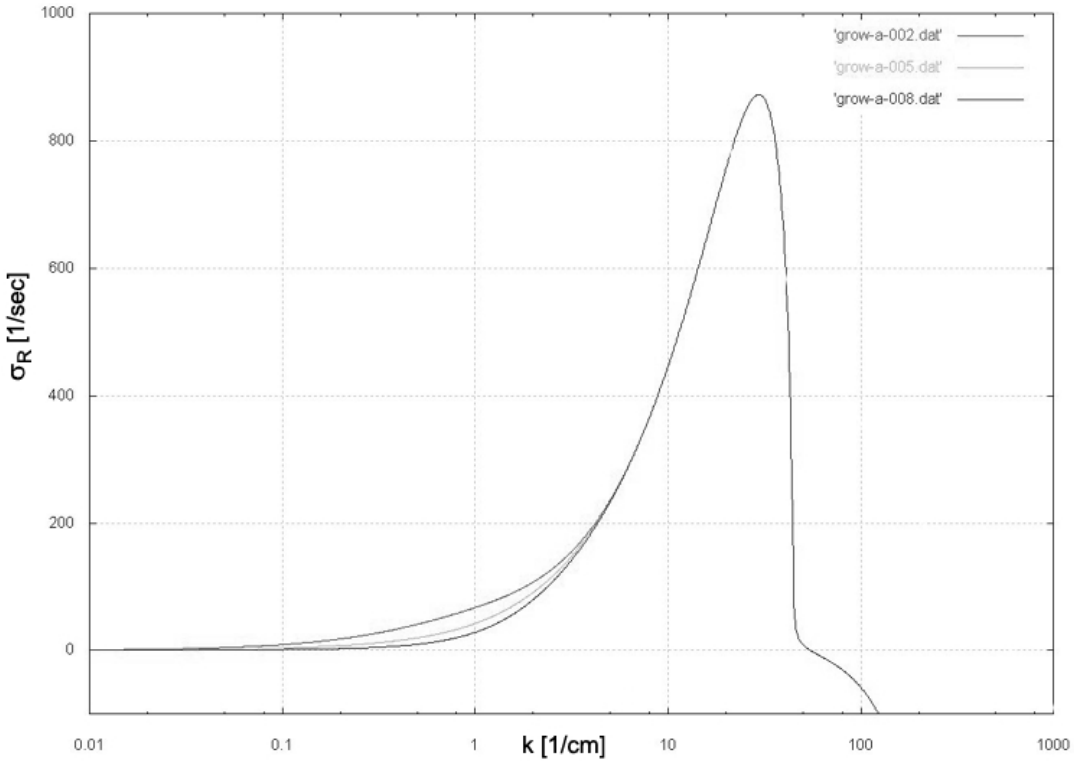

Figure 5a. $\hat{\mu} = 0.018$ *(water,* $\mu_l = 1$ *cp).* $V = 1500$ *cm/sec. The graphs are top to bottom* $\alpha = 0.2,\ 0.5,\ 0.8$.

$\hat{h}_a$	$k_m[1/cm]$	$\lambda_m[cm]$	$\sigma_{Rm}[1/sec]$	$\tilde{C}_{Rm}[cm/sec]$
0.01	*29.9016*	*0.2101*	*1447.9245*	*3.0442*
0.1	*29.6635*	*0.2118*	*872.5395*	*2.0488*
0.2	*29.6635*	*0.2118*	*872.5387*	*2.0488*
0.3	*29.6635*	*0.2118*	*872.5387*	*2.0488*
0.4	*29.6635*	*0.2118*	*872.5387*	*2.0488*
0.5	*29.6635*	*0.2118*	*872.5387*	*2.0488*
0.6	*29.6635*	*0.2118*	*872.5387*	*2.0488*
0.7	*29.6635*	*0.2118*	*872.5387*	*2.0488*
0.8	*29.6635*	*0.2118*	*872.5387*	*2.0488*
0.9	*29.6635*	*0.2118*	*872.5385*	*2.0488*
0.99	*32.1325*	*0.1955*	*706.1702*	*1.4543*

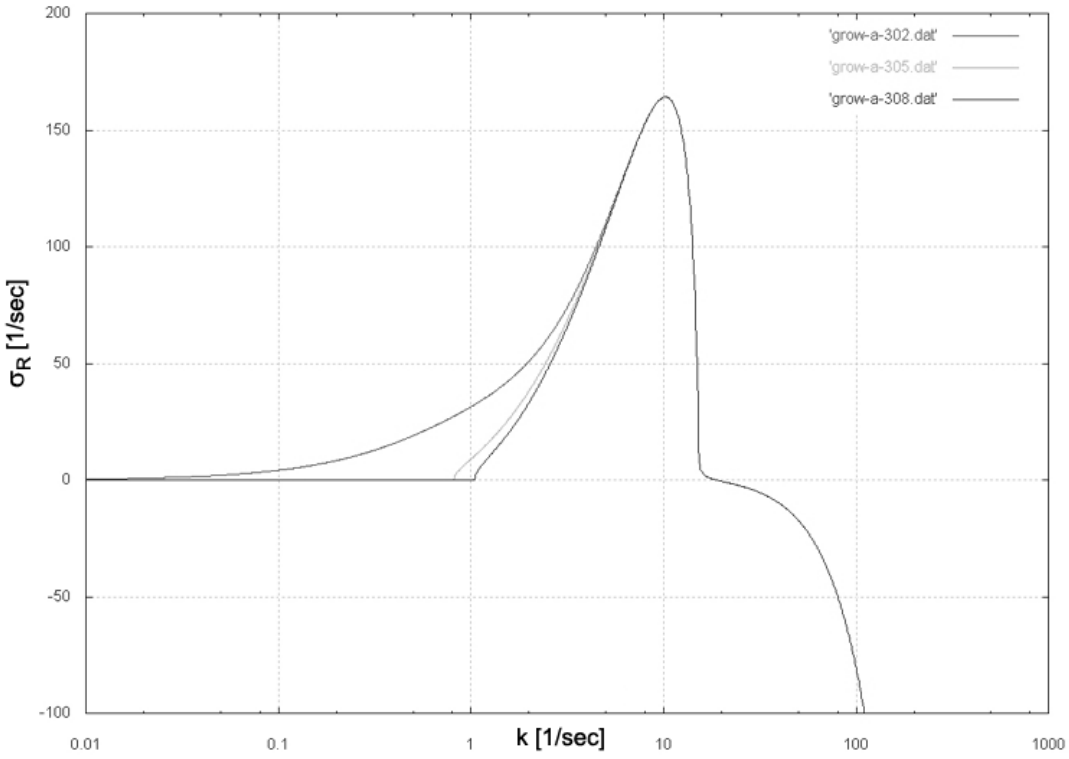

Figure 5b. $\hat{\mu} = 0.018$, $V = 900$ $cm/sec.$

$\hat{h}_a$	$k_m[1/cm]$	$\lambda_m[cm]$	$\sigma_{Rm}[1/sec]$	$\tilde{C}_{Rm}[cm/sec]$
0.01	*15.3993*	*0.4080*	*615.3088*	*3.0461*
0.1	*10.0000*	*0.6283*	*167.7322*	*1.1827*
0.2	*10.2428*	*0.6134*	*164.2430*	*1.1745*
0.3	*10.2428*	*0.6134*	*164.2245*	*1.1744*
0.4	*10.2428*	*0.6134*	*164.2244*	*1.1744*
0.5	*10.2428*	*0.6134*	*164.2244*	*1.1744*
0.6	*10.2428*	*0.6134*	*164.2244*	*1.1744*
0.7	*10.2428*	*0.6134*	*164.2243*	*1.1744*
0.8	*10.2428*	*0.6134*	*164.2194*	*1.1744*
0.9	*10.3250*	*0.6085*	*163.3315*	*1.1642*
0.99	*11.3646*	*0.5529*	*84.6599*	*0.3670*

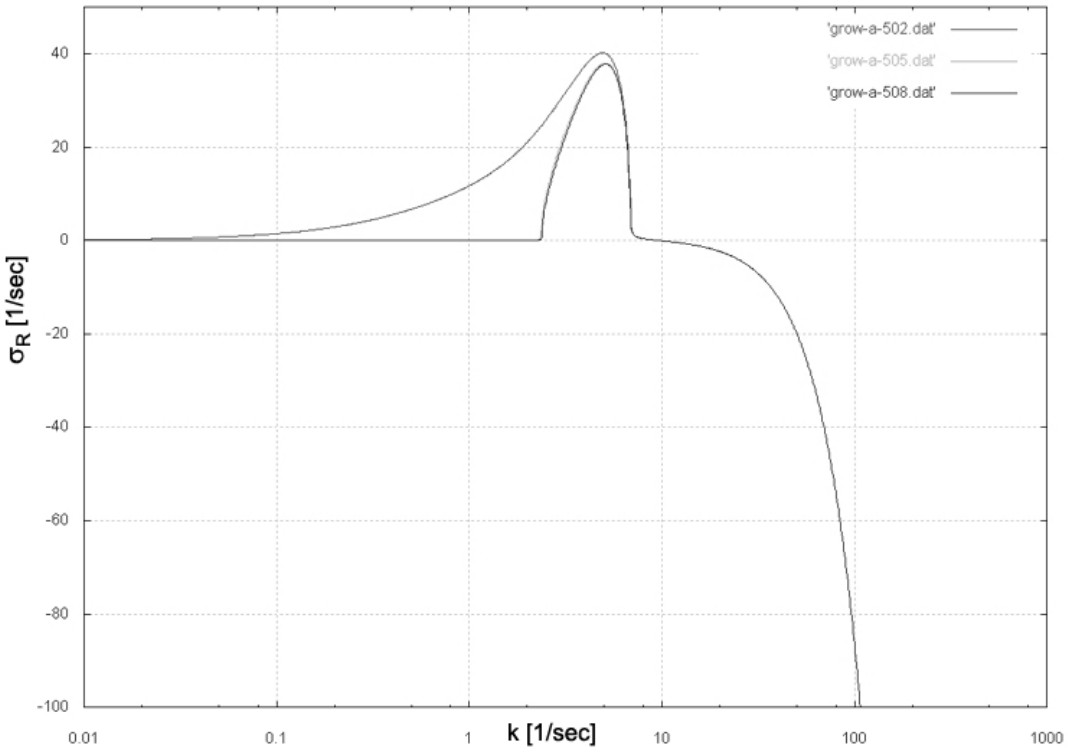

Figure 5c. $\hat{\mu} = 0.018$, $V = 680$ *cm/sec.*

$\hat{h}_a$	$k_m[1/cm]$	$\lambda_m[cm]$	$\sigma_{Rm}[1/sec]$	$\tilde{C}_{Rm}[cm/sec]$
0.01	*11.1844*	*0.5618*	*391.3929*	*3.0669*
0.1	*4.5680*	*1.3755*	*62.1098*	*1.0388*
0.2	*4.9088*	*1.2800*	*40.1792*	*0.8951*
0.3	*5.0683*	*1.2397*	*38.1441*	*0.8920*
0.4	*5.0683*	*1.2397*	*37.9928*	*0.8916*
0.5	*5.0683*	*1.2397*	*37.9811*	*0.8916*
0.6	*5.0683*	*1.2397*	*37.9791*	*0.8915*
0.7	*5.0683*	*1.2397*	*37.9636*	*0.8908*
0.8	*5.1090*	*1.2298*	*37.7670*	*0.8834*
0.9	*5.2330*	*1.2007*	*35.3134*	*0.7846*
0.99	*5.4030*	*1.1629*	*13.7411*	*0.1437*

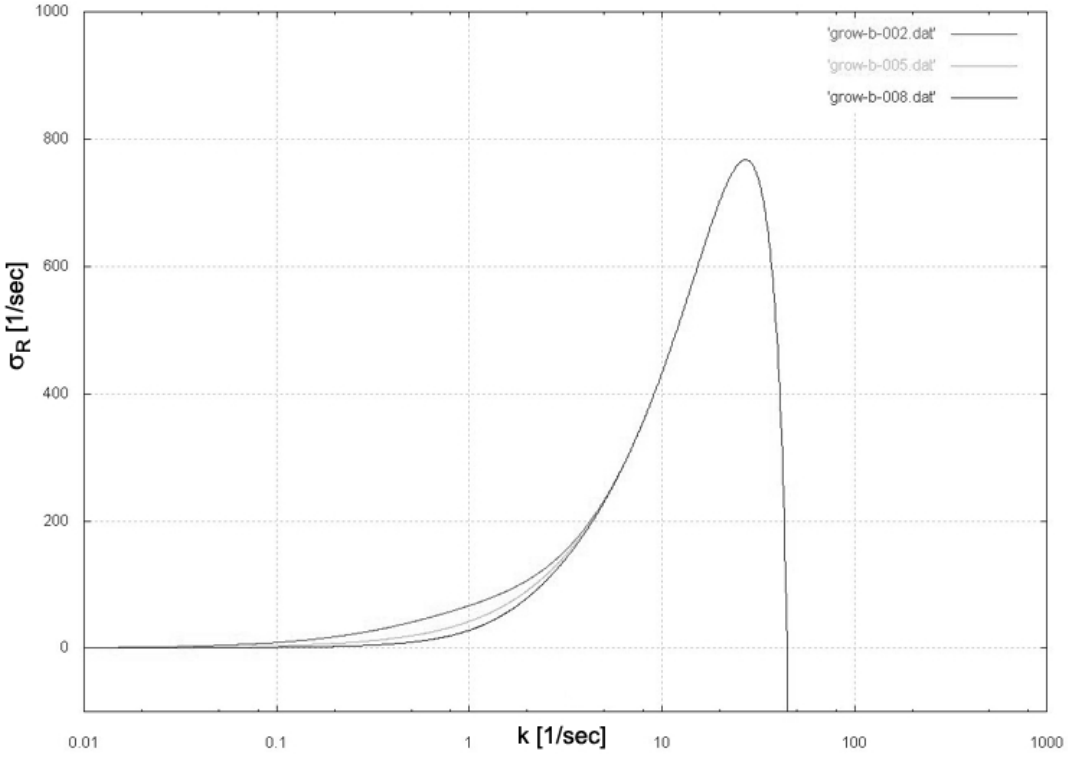

Figure 6a. $\hat{\mu} = \hat{\rho} = 0.0012$ *(μ_l = 15 cp, inviscid).* $V = 1500$ *cm/sec. The graphs are top to bottom* $\alpha = 0.2,\ 0.5,\ 0.8$.

$\hat{h}_a$	$k_m[1/cm]$	$\lambda_m[cm]$	$\sigma_{Rm}[1/sec]$	$\tilde{C}_{Rm}[cm/sec]$
0.01	*26.9498*	*0.2331*	*1339.8608*	*3.0219*
0.1	*27.1661*	*0.2313*	*767.9639*	*1.7978*
0.2	*27.1661*	*0.2313*	*767.9616*	*1.7978*
0.3	*27.1661*	*0.2313*	*767.9616*	*1.7978*
0.4	*27.1661*	*0.2313*	*767.9616*	*1.7978*
0.5	*27.1661*	*0.2313*	*767.9616*	*1.7978*
0.6	*27.1661*	*0.2313*	*767.9616*	*1.7978*
0.7	*27.1661*	*0.2313*	*767.9616*	*1.7978*
0.8	*27.1661*	*0.2313*	*767.9616*	*1.7978*
0.9	*27.1661*	*0.2313*	*767.9607*	*1.7978*
0.99	*30.1416*	*0.2085*	*584.7287*	*1.1590*

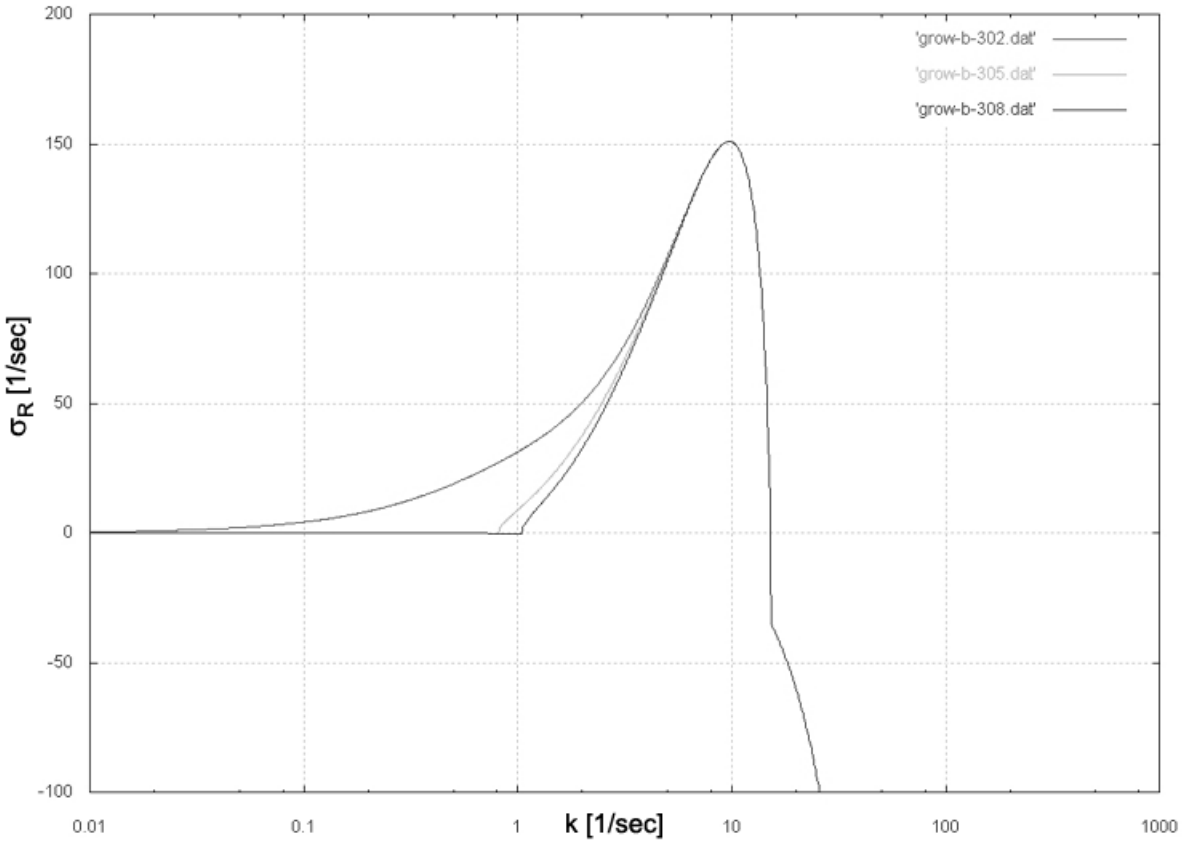

Figure 6b. $\hat{\mu} = \hat{\rho} = 0.0012$, $V = 900$ *cm/sec.*

$\hat{h}_a$	$k_m[1/cm]$	$\lambda_m[cm]$	$\sigma_{Rm}[1/sec]$	$\tilde{C}_{Rm}[cm/sec]$
0.01	*14.4452*	*0.4350*	*585.2220*	*3.0640*
0.1	*9.4557*	*0.6645*	*155.1119*	*1.0965*
0.2	*9.6853*	*0.6487*	*151.0123*	*1.0788*
0.3	*9.6853*	*0.6487*	*150.9832*	*1.0787*
0.4	*9.6853*	*0.6487*	*150.9830*	*1.0787*
0.5	*9.6853*	*0.6487*	*150.9830*	*1.0787*
0.6	*9.6853*	*0.6487*	*150.9830*	*1.0787*
0.7	*9.6853*	*0.6487*	*150.9829*	*1.0787*
0.8	*9.7630*	*0.6436*	*150.9749*	*1.0786*
0.9	*9.8414*	*0.6384*	*149.8546*	*1.0643*
0.99	*10.6605*	*0.5894*	*69.5887*	*0.2854*

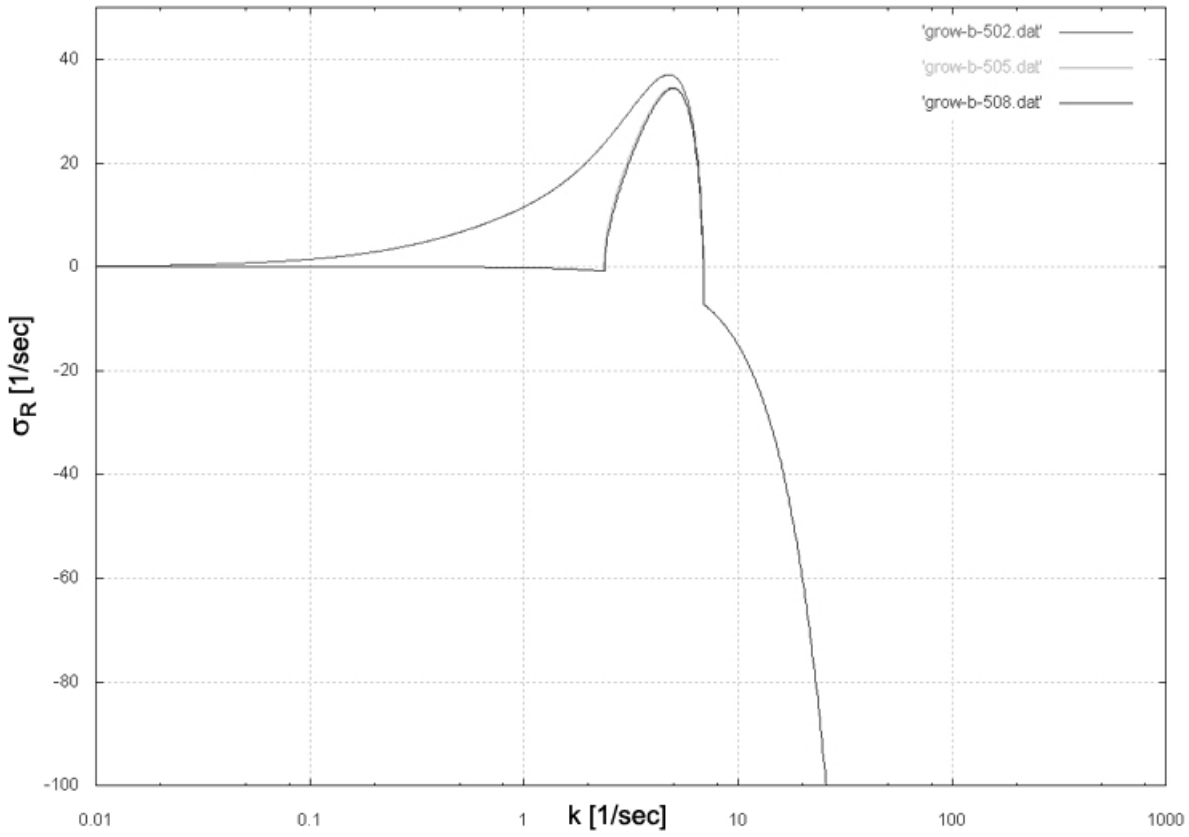

Figure 6c. $\hat{\mu} = \hat{\rho} = 0.0012$, $V = 680$ *cm/sec.*

$\hat{h}_a$	$k_m[1/cm]$	$\lambda_m[cm]$	$\sigma_{Rm}[1/sec]$	$\tilde{C}_{Rm}[cm/sec]$
0.01	*10.5756*	*0.5941*	*375.3248*	*3.0963*
0.1	*4.3540*	*1.4431*	*59.4019*	*1.0152*
0.2	*4.7543*	*1.3216*	*37.0645*	*0.8281*
0.3	*4.9088*	*1.2800*	*34.8433*	*0.8159*
0.4	*4.9482*	*1.2698*	*34.6673*	*0.8151*
0.5	*4.9482*	*1.2698*	*34.6533*	*0.8150*
0.6	*4.9482*	*1.2698*	*34.6507*	*0.8150*
0.7	*4.9482*	*1.2698*	*34.6323*	*0.8142*
0.8	*4.9879*	*1.2597*	*34.4071*	*0.8048*
0.9	*5.1090*	*1.2298*	*31.8165*	*0.7020*
0.99	*5.1500*	*1.2200*	*10.4457*	*0.1061*

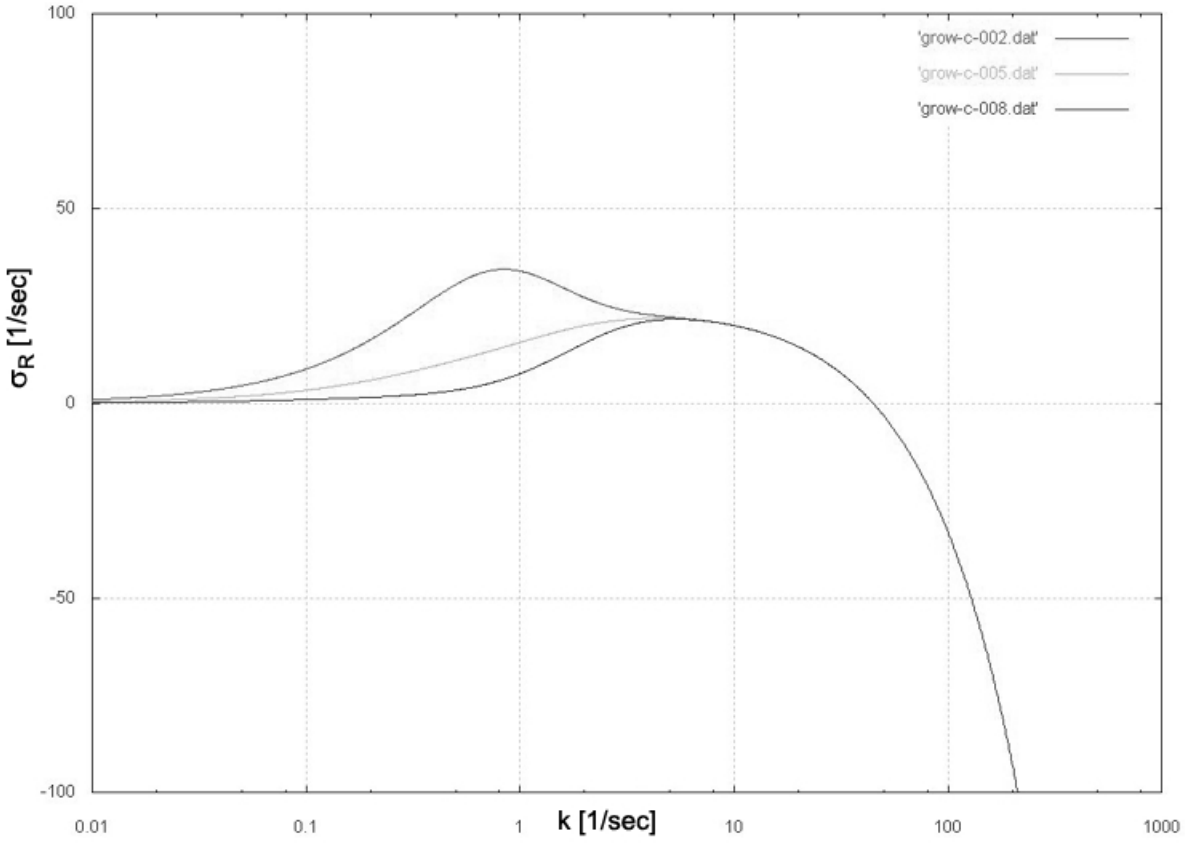

Figure 7a. $\hat{\mu} = 3.6 \times 10^{-6}$ *($\mu_l = 50$ p). $V = 1500$ cm/sec. The graphs are top to bottom* $\alpha = 0.2,\ 0.5,\ 0.8$.

$\hat{h}_a$	$k_m[1/cm]$	$\lambda_m[cm]$	$\sigma_{Rm}[1/sec]$	$\tilde{C}_{Rm}[cm/sec]$	
0.01	*1.8214*	*3.4496*	*295.1267*	*24.5529*	
0.1	*0.9158*	*6.8608*	*60.0383*	*4.4949*	
0.2	*0.8454*	*7.4318*	*34.4319*	*2.0489*	
0.3	*0.9380*	*6.6982*	*24.0840*	*0.9710*	*max*
0.3	*3.0873*	*2.0352*	*21.9598*	*0.0860*	*min*
0.3	*3.8312*	*1.6400*	*21.9726*	*0.0579*	*max*
0.4	*4.4242*	*1.4202*	*21.8929*	*0.0447*	
0.5	*4.4597*	*1.4089*	*21.8867*	*0.0440*	
0.6	*4.4955*	*1.3977*	*21.8818*	*0.0434*	
0.7	*4.6788*	*1.3429*	*21.8456*	*0.0404*	
0.8	*5.3600*	*1.1722*	*21.6053*	*0.0317*	
0.9	*7.7426*	*0.8115*	*20.2113*	*0.0168*	
0.99	*20.5353*	*0.3060*	*6.8007*	*0.0029*	

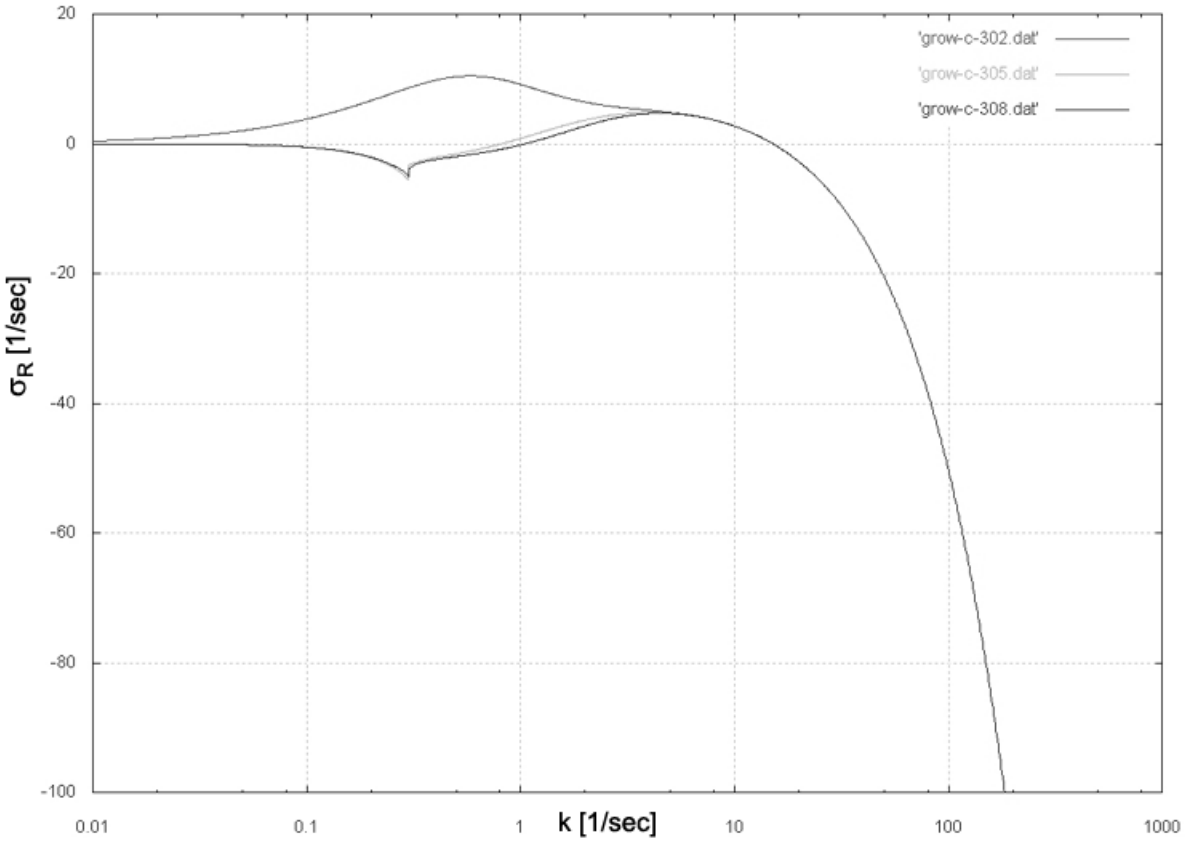

Figure 7b. $\hat{\mu} = 3.6 \times 10^{-6}$, $V = 900$ *cm/sec.*

$\hat{h}_a$	$k_m[1/cm]$	$\lambda_m[cm]$	$\sigma_{Rm}[1/sec]$	$\tilde{C}_{Rm}[cm/sec]$	
0.01	*1.3229*	*4.7495*	*145.8908*	*19.6444*	
0.1	*0.6759*	*9.2965*	*24.7985*	*3.0174*	
0.2	*0.5806*	*10.8216*	*10.4837*	*1.1994*	
0.3	*0.8387*	*7.4915*	*4.2952*	*0.1928*	*max*
0.3	*0.9841*	*6.3845*	*4.2938*	*0.1348*	*min*
0.3	*3.7704*	*1.6664*	*4.9068*	*0.0107*	*max*
0.4	*4.0195*	*1.5632*	*4.8637*	*0.0097*	
0.5	*4.0517*	*1.5507*	*4.8589*	*0.0096*	
0.6	*4.0842*	*1.5384*	*4.8561*	*0.0095*	
0.7	*4.1501*	*1.5140*	*4.8401*	*0.0092*	
0.8	*4.4597*	*1.4089*	*4.7346*	*0.0082*	
0.9	*5.5342*	*1.1353*	*4.0999*	*0.0054*	
0.99	*7.9943*	*0.7860*	*0.7409*	*0.0007*	

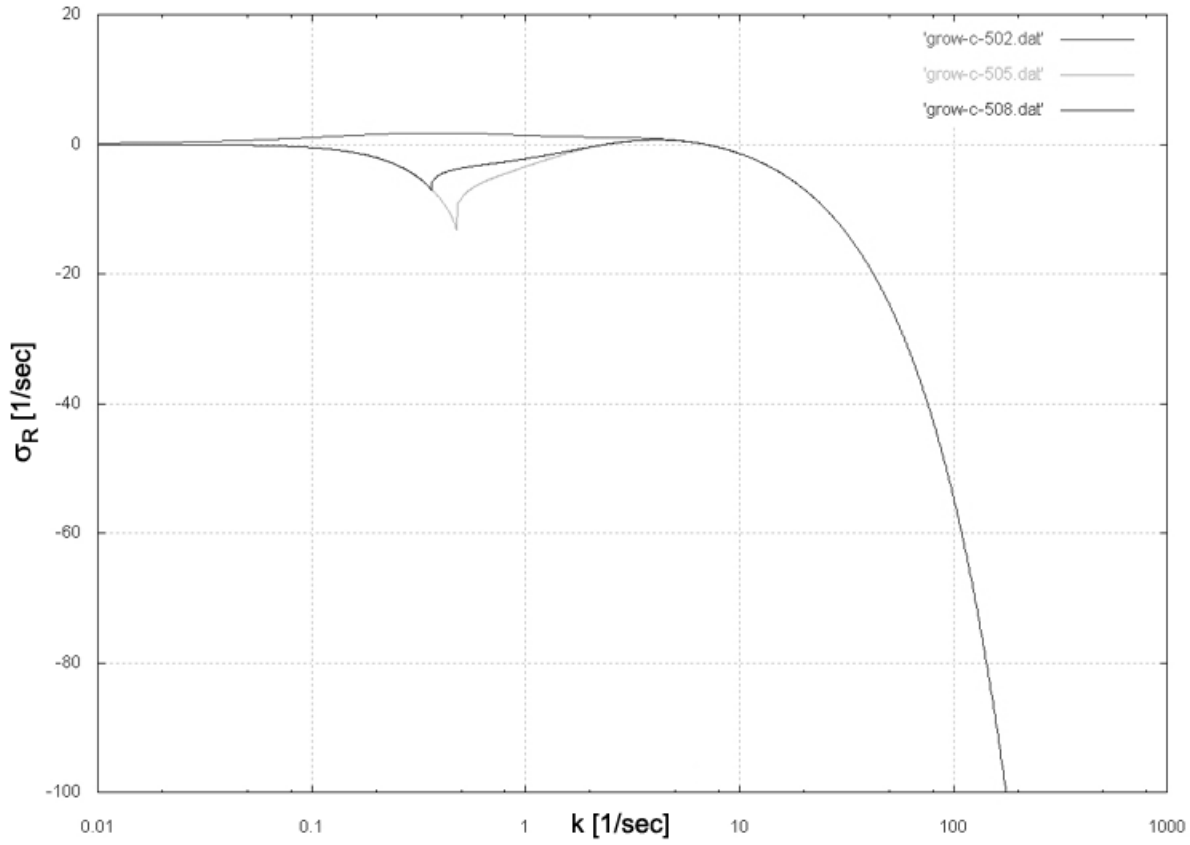

Figure 7c. $\hat{\mu} = 3.6 \times 10^{-6}$, $V = 680$ *cm/sec.*

$\hat{h}_a$	$k_m[1/cm]$	$\lambda_m[cm]$	$\sigma_{Rm}[1/sec]$	$\tilde{C}_{Rm}[cm/sec]$
0.01	*1.1184*	*5.6178*	*97.9687*	*17.0073*
0.1	*0.5579*	*11.2629*	*12.8802*	*2.2460*
0.2	*0.3893*	*16.1399*	*1.7726*	*0.5285*
0.3	*3.8929*	*1.6140*	*0.7278*	*0.0032*
0.4	*4.0195*	*1.5632*	*0.7047*	*0.0032*
0.5	*4.0517*	*1.5507*	*0.7019*	*0.0031*
0.6	*4.0517*	*1.5507*	*0.7013*	*0.0031*
0.7	*4.0517*	*1.5507*	*0.6987*	*0.0031*
0.8	*4.1170*	*1.5261*	*0.6797*	*0.0030*
0.9	*4.3193*	*1.4547*	*0.5523*	*0.0023*
0.99	*4.6046*	*1.3645*	*0.0769*	*0.0003*

6 Comparison of theory and experiments in rectangular ducts

Kordyban and Ranov [KD] 1970 and Wallis and Dobson [WD] 1973 are the only authors to report the results of experiments in rectangular ducts. Many other experiments have been carried out in round pipes; the results of these experiments are not perfectly matched to the analysis done here or elsewhere, and will be discussed later.

All experimenters are motivated to understand the transition from stratified flow with a flat smooth interface to slug flow. They note that in many cases the first transition, which is studied

here, is from smooth stratified flow to small amplitude sinusoidal waves called capillary waves by [WD]. The data given by these authors is framed as a transition to slug flow, though the criteria given are for the loss of stability of smooth stratified flow. The theoretical predictions are for the loss stability, which may or may not be to slug flow.

Finally we call the reader's attention to the fact that all the linear theories that neglect viscosity overpredict the observed stability limit. [WD] note that "..as a result of the present experiments it is our view that the various small wave theories are all inappropriate for describing 'slugging.' Slugging is the result of the rapid development of a large wave which rides over the underlying liquid and can eventually fill the channel to form a slug..." [WD] also note that "It was found possible to produce slugs at air fluxes less than those predicted" by their empirical formula, $j^* < 0.5\alpha^{3/2}$. All this suggests that we may be looking at something akin to subcritical bifurcation with multiple solutions and hysteresis.

Turning next to linearized theory we note that [WD] do an inviscid analysis stating that "...if waves are 'long' ($kh_L \ll, kh_G \ll 1$) and surface tension can be neglected, the predicted instability condition is

$$(v_G - v_L)^2 > (\rho_L - \rho_G)\, g \left(\frac{h_G}{\rho_G} + \frac{h_L}{\rho_L} \right). \quad (6.1)$$

If $\rho_G \ll \rho_L$ and $v_L \ll v_G$ they may be simplified further to give

$$\rho_G v_G^2 > g(\rho_L - \rho_G) h_G \quad (6.2)$$

which is the same as

$$j_G^* > \alpha^{3/2} \quad (6.3)$$

..." Here $\alpha = h_G/H$ and

$$j_G^* = \frac{v_G \alpha \sqrt{\rho_G}}{\sqrt{gH(\rho_L - \rho_G)}} > \alpha^{3/2}.$$

Their criterion (6.1) is identical to our (4.6) for the long wave inviscid case $\hat{\mu} = \hat{\rho}$ and $\hat{k} \to 0$. They compare their criterion (6.3) with transition observations that they call "slugging" and note that empirically the stability limit is well described by

$$j_G^* > 0.5\alpha^{3/2},$$

rather than (6.3).

In figures 8 and 9 we plotted j^* vs. α giving $j_G^* = \alpha^{3/2}$ and $0.5\alpha^{3/2}$. In figure 8 we give the results from our viscous potential flow theory for the inviscid case in table 2 and the air water case in table 1. In figure 9 we show the experimental results presented by [WD] and [KR]. Our theory fits the data better than [WD] $j^* = \alpha^{3/2}$; it still overpredicts the data for small α but fits the large α data quite well; we have good agreement when the water layer is small.

The predicted wave length and wave speed in table 1 can be compared with experiments in principle, but in practice this comparison is obscured by the focus on the formation of slugs. For example, [WD] remards that "at a certain minimum air velocity, ripples appeared at the air entry end, and slowly spread down the channel. These waves were about 2-in. (0.05m) long and were made up of long wave crests, with three or four capillary waves riding on the troughs. The long waves traveled faster than the capillary waves." The speed of these long waves were reported by [WD] to be less than 0.3 m/sec in all cases. Theoretical results from table 1 show that the wave length λ_c increases with the water depth (as in the experiment) and the wave speed varies from 0.1 m/sec to 0.04 m/sec. The predicted spacing of the waves on average is about 1.5 cm/sec. *The predicted wave length and wave speed from viscous potential flow are apparently in good agreement with the waves [WD] call capillary waves.*

Observations similar to those of [WD] just cited were made by Andritsos, Williams and Hanratty [AWH] 1989 who note that for high viscosity liquid (80 cp) a region of regular 2D waves barely exists. "The first disturbances observed with increasing gas velocity are small-amplitude, small-wavelength, rather regular 2D waves. With a slight increase in gas velocity, these give way to a few large-amplitude waves with steep fronts and smooth troughs, and with spacing that can vary from a few centimeters to a meter."

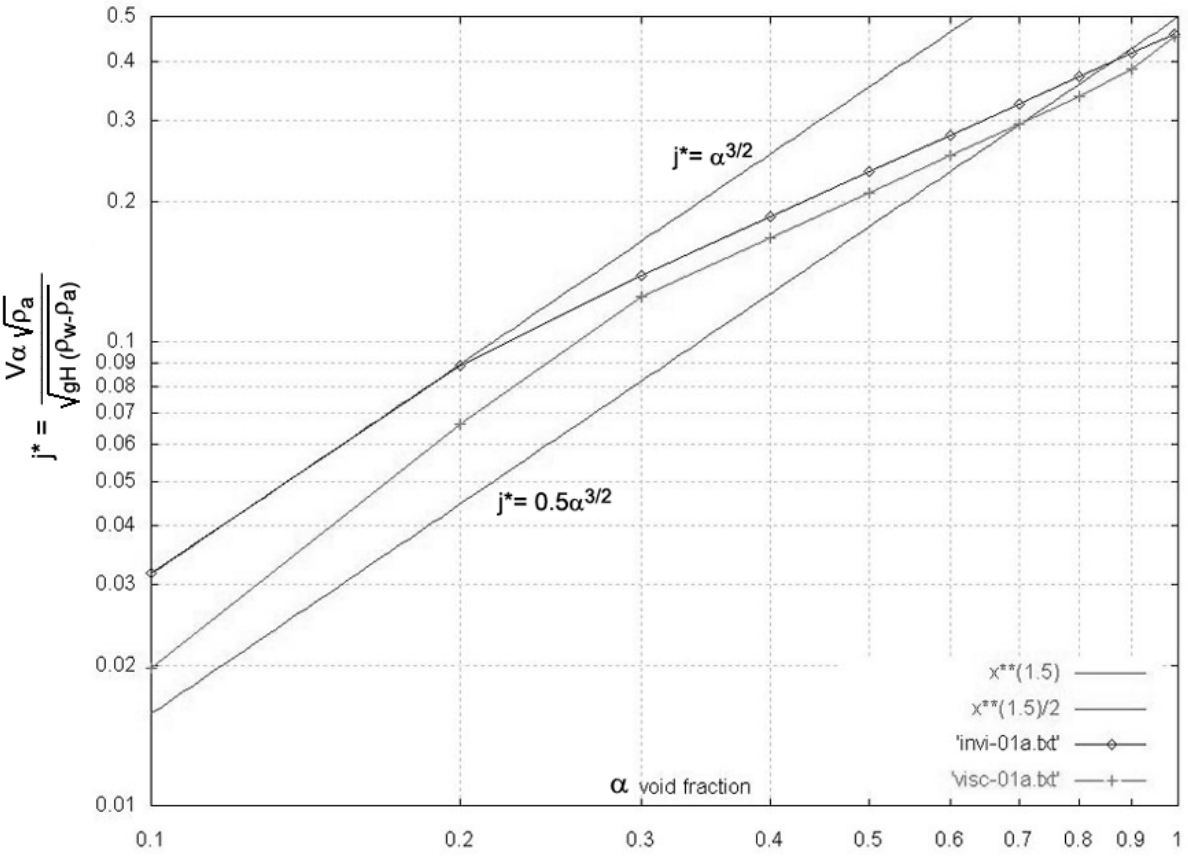

Figure 8: *j^* vs. α for marginal stability of air and water in a frame in which the water velocity is zero. $\diamond$ = inviscid fluid from table 2; $+$ = air-water with $\gamma = 60$ dynes/cm from table 1. Surface tension γ is important.*

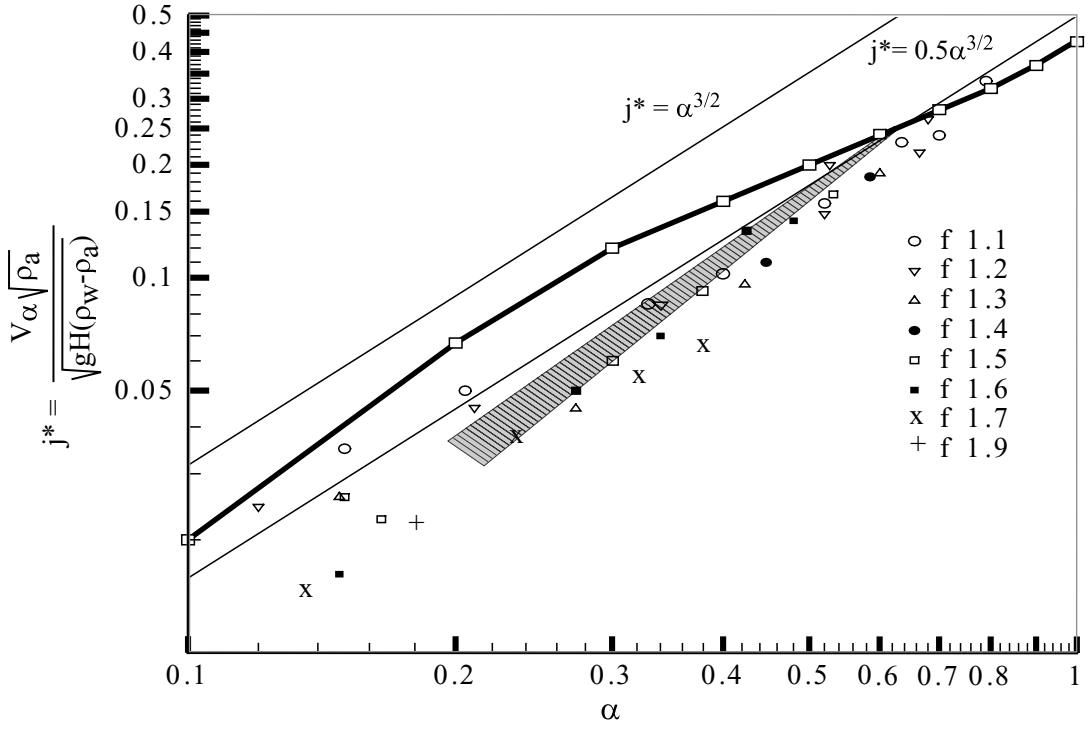

Figure 9: *j^* vs. α. Comparison of theory and experiments. $j^* = \alpha^{3/2}$ is the long wave criterion for an inviscid fluid put forward by Wallis and Dobson 1973. $j^* = 0.5\alpha^{3/2}$ was proposed by them as best fit to the experiments $f1.1$ through $f1.9$ described in their paper. The shaded region is from experiments by Kordyban and Ranov 1970. The heavy line □ is our result for air-water from table 1.*

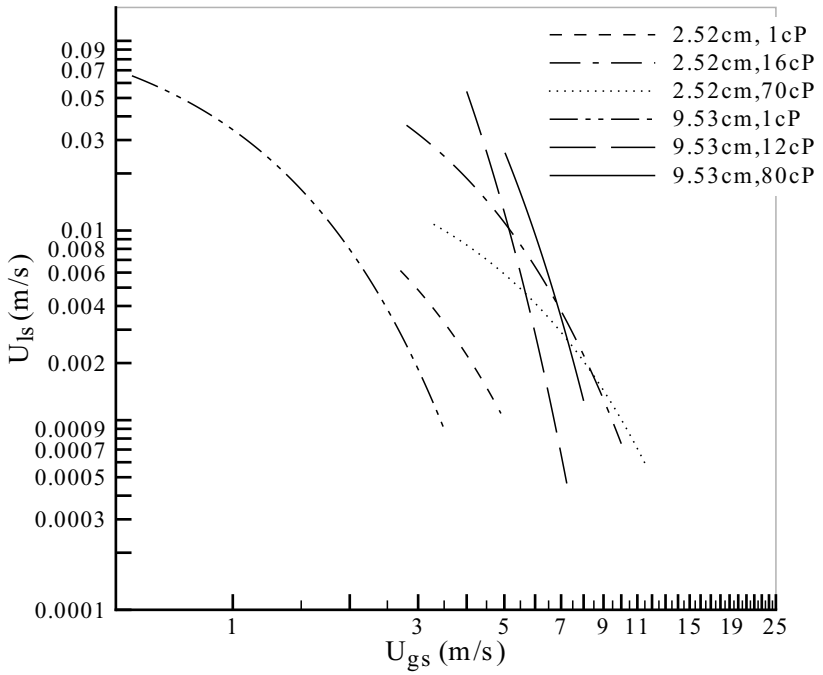

Figure 10: *(After Andritsos and Hanratty 1987.) These lines represent the borders between smooth stratified flow and disturbed flow observed in experiment. The water-air data is well below the cluster of high viscosity data that is bunched together.*

7 Critical viscosity and density ratios

The most interesting aspect of our potential flow analysis is the surprising importance of the viscosity ratio $\hat{\mu} = \mu_a/\mu_l$ and density ratio $\hat{\rho} = \rho_a/\rho_l$; when $\hat{\mu} = \hat{\rho}$ the equation (4.2) for marginal stability is identical to the equation for the neutral stability of an inviscid fluid even though $\hat{\mu} = \hat{\rho}$ in no way implies that the fluids are inviscid. Moreover, the critical velocity is a maximum at $\hat{\mu} = \hat{\rho}$; hence the critical velocity is smaller for *all* viscous fluids such that $\hat{\mu} \neq \hat{\rho}$ and is smaller than the critical velocity for inviscid fluids. All this may be understood by inspection of figure 4, which shows that $\hat{\mu} = \hat{\rho}$ is a distinguished value that can be said to divide high viscosity liquids with $\hat{\mu} < \hat{\rho}$ from low viscosity liquids. As a practical matter the stability limit of high viscosity liquids can hardly be distinguished from each other while the critical velocity decreases sharply for low viscosity fluids.

The condition $\hat{\mu} = \hat{\rho}$ can be written as

$$\mu_l = \mu_a \frac{\rho_l}{\rho_a}. \tag{7.1}$$

For air and water

$$\mu_l = 0.15 \,\text{poise}. \tag{7.2}$$

Hence $\mu_l > 0.15$ poise is a high viscosity liquid and $\mu_l < 0.15$ poise is a low viscosity liquid provided that $\rho_l \approx 1\text{gm/cm}^3$.

Other authors have noted strange relations between viscous and inviscid fluids. Barnea and Taitel [BT] 1993 note that "the neutral stability lines obtained from the viscous Kelvin-Helmholtz analysis and the inviscid analysis are quite different for the case of low liquid viscosities, whereas they are quite similar for high viscosity, contrary to what one would expect." Their analysis starts from a two-fluid model and it leads to different dispersion relations; they do not obtain the critical condition $\hat{\mu} = \hat{\rho}$. Earlier, Andritsos *et al* [AWH] noted a "surprising result that the invis-

cid theory becomes more accurate as the liquid viscosity increases."

Andritsos and Hanratty [AH] have presented flow regime maps for pipe flows in 2.52 cm and 9.53 cm pipe for fluids of different viscosity ranging from 1 cp to 80 cp. These figures present flow boundaries; the boundaries of interest to us are those that separate "smooth" flow from disturbed flow. Liquid holdups (essentially α) are not specified in these experiments. We extracted the smooth flow boundaries from figures in [AH] and collected them in our figure 10. It appears from this figure that the boundaries of smooth flow for all the liquids with $\mu_l > 15$ cp are close together, but the boundary for water with $\mu_l = 1$ cp is much lower. The velocities shown in these figures are superficial velocities; the average velocities which could be compared with critical velocities in tables 1, 2 and 3 are larger than the superficial velocities and are significantly larger than those in the tables.

8 Further comparisons with previous results

As a practical matter interest in the pipelining of gas-liquid flow is in round pipes. All experiments other than those of [KR] amd [WD] reviewed in section 6 have been done in round pipes. To our knowledge there is no other theoretical study in which the stability of stratified flow in a round pipe is studied without approximations. Theoretical studies of stability of stratified flow have been presented by Wallis [W] 1969; Wu, Pots, Hollenberg and Meerhoff [WPHM] 1987, Barnea [B] 1991, Crowley, Wallis and Barry [CWB] 1992, Kordyban and Ranov [KR] 1970, Wallis and Dobson [WD] 1973, Taitel and Dukler [TD] 1976, Mishima and Ishii [MI] 1980, Lin and Hanratty [LH] 1986, Andritsos and Hanratty [AH] 1987, Andritsos, Williams and Hanratty [AWH] 1989, Barnea and Taitel [BT] 1993. Viscosity is neglected by [KR], [WD], [TD] and [MI]. Surface tension is neglected by [W], [KR], [WD], [TD], [MI] and [LH]. [W], [LH], [WPHM], [B], [CWB] and [BT] use one or another of the forms of two fluids equations. In these equations averaged variables are introduced, the actual geometry is represented only so far as its area and round, elliptical or rectangular pipes with equal areas are equivalent. The effects of viscosity in these averaged models are introduced through empirical wall and interfacial fraction correlations. All these authors neglect the normal component of viscous stress (extensional stresses are neglected). The approach of [AH], [AWH] is different; all the main physical effects are represented in analysis of the plane flow which is later applied to flow in round pipes. The disturbuance equations for the liquid are solved exactly except that the shear of basic liquid flow is neglected using a plug flow assumption. The effects of the gas on the liquid are represented through empirical correlations and further approximations are required for round pipes.

Experiments on the stability of stratified flow have been reported by [KR], [WD], [TD], [LH], [CWB] and [AH]. The experiments of [LH] and [AH] do not have data giving the height of the liquid and gas layers. Kordyban & Ranov [KR] and Wallis & Dobson [WD] did experiments in rectangular ducts, the geometry analyzed in this paper, the other experiments were done in round pipes. Authors [LH], [CWB] and [AH] are the only experimenters to report results for fluids with different viscosities.

There is difficulty in comparing the results of experiments in round pipes and rectangular channels. The common practice for round pipes is to express results in terms of h/D where D is the pipe diameter and h is the height above the bottom of the pipe; h/H is the liquid fraction in rectangular pipes and $\alpha = 1 - h/H$ is the gas fraction, but h/D is not the liquid fraction in round pipes and $1 - h/D$ is not the gas fraction in round pipes. [LH] presented experimental results for thin liquid films in round pipes giving (their figure 4) $h/Dvs.j*$; we converted their results to $j * vs.1 - h/D$ and compared them in figure 11 with the results given in figure 9. The experimental results for round pipes are much lower than those for rectangular pipes. All this points to the necessity of taking care when comparing results between round and retangular pipes and inter-

preting results of analysis for one experiment to the other.

9 Nonlinear effects

There is no theory which is faithful to all conditions at play in experiments. None of the theories agree with experiments. Attempts to represent the effects of viscosity are only partial, as in our theory of viscous potential flow, or they require empirical data on wall and interfacial friction, which are not known exactly and may be adjusted to fit the data. Some choices for empirical inputs underpredict and others overpredict the experimental data.

It is widely acknowledged that nonlinear effects at play in the transition from stratified to slug flow are not well understood. The well-known criteria of Taitel and Dukler 1976, based on a heuristic adjustment of the linear inviscid long wave theory for nonlinear effects, is possible the most accurate predictor of experiments. Their criterion replaces $j* = \alpha^{3/2}$ with $j* = \alpha^{5/2}$. We can obtain the same heuristic adjustment for nonlinear effects on viscous potential flow by multiplying the critical value of velocity in table 1 by α. Plots of $j* = \alpha^{3/2}$, $j* = \alpha^{5/2}$ and the heuristic adjustment of viscous potential flow, together with the experimental values of [WD] and [KR] are shown in figure 12. The good agreements in evidence there lacks a convincing foundation.

10 Conclusion

We studied Kelvin-Helmholtz stability of superposed uniform streams in rectangular ducts using viscous potential flow. Viscous potential flows satisfy the Navier-Stokes equations. Because the no-slip condition can not be satisfied the effects of shear stresses are neglected, but the effects of extensional stresses at the interface on the normal stresses are fully represented. The solution presented is complete and mathematically rigorous. The effects of shear stresses are neglected at the outset; after that no empirical inputs are introduced. The main result of the analysis is the emergence of a critical value of velocity, discussed in the paper abstract and in section 7. The main consequence of this result is that for air-liquid systems the critical values of velocity for liquids greater than 15 cp are essentially independent of viscosity and the same as for an inviscid fluid, but for liquids with viscosities less than 15 cp the stability limits are much lower. The criterion for stability of stratified flow given by viscous potential flow is in good agreement with experiments when the liquid layer is thin, but it overpredicts the data when the liquid layer is thick. Though viscous potential flow neglects important effects of shear the qualitative prediction of the peculiar effects of liquid viscosity has been obtained by other authors using other methods of analysis.

A rather accurate predictor of experimental results is given by applying the nonlinear correction factor to account for the effect of finite amplitude wave on the results of viscous potential flow.

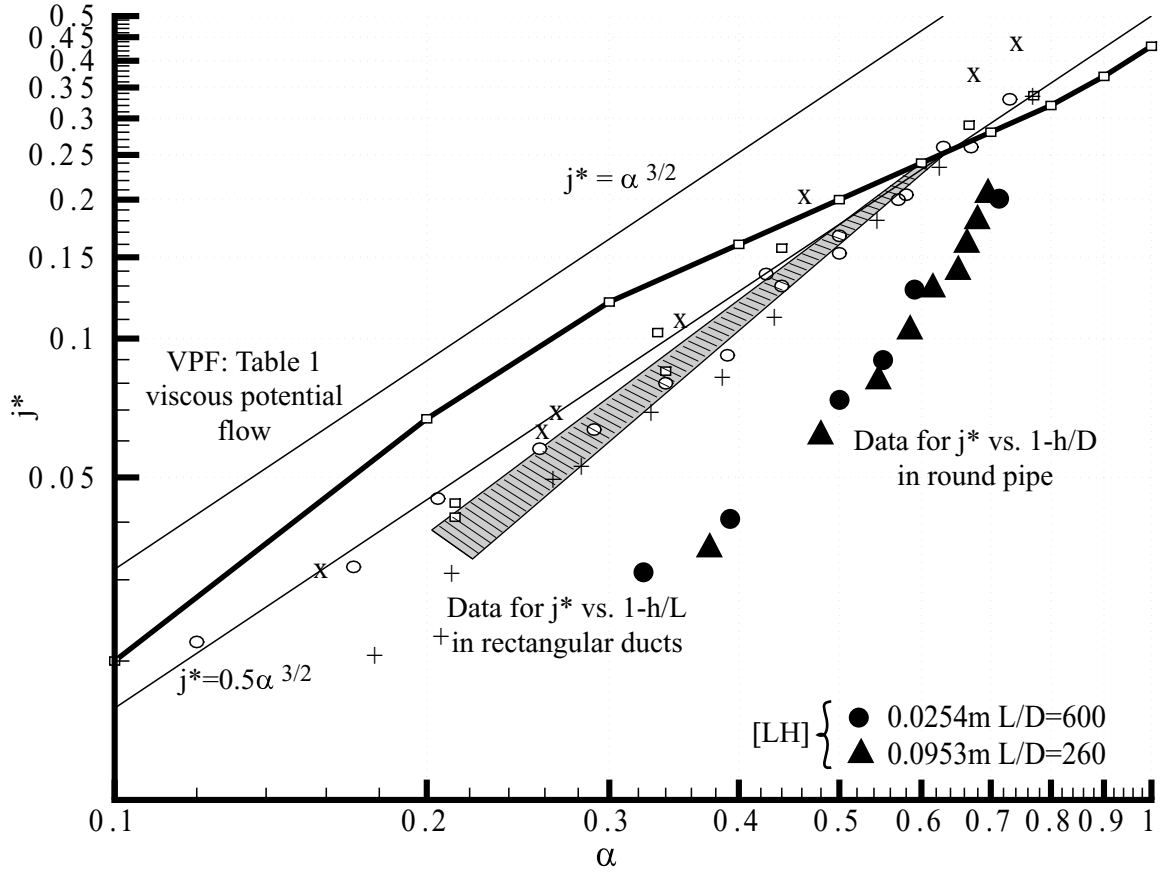

Figure 11: *Comparison of experimental data in rectangular conduits $j* vs. 1 - h/H = \alpha$ and in round pipes $j* vs. 1 - h/D = \alpha$ (Lin & Hanratty 1986, figure 4).*

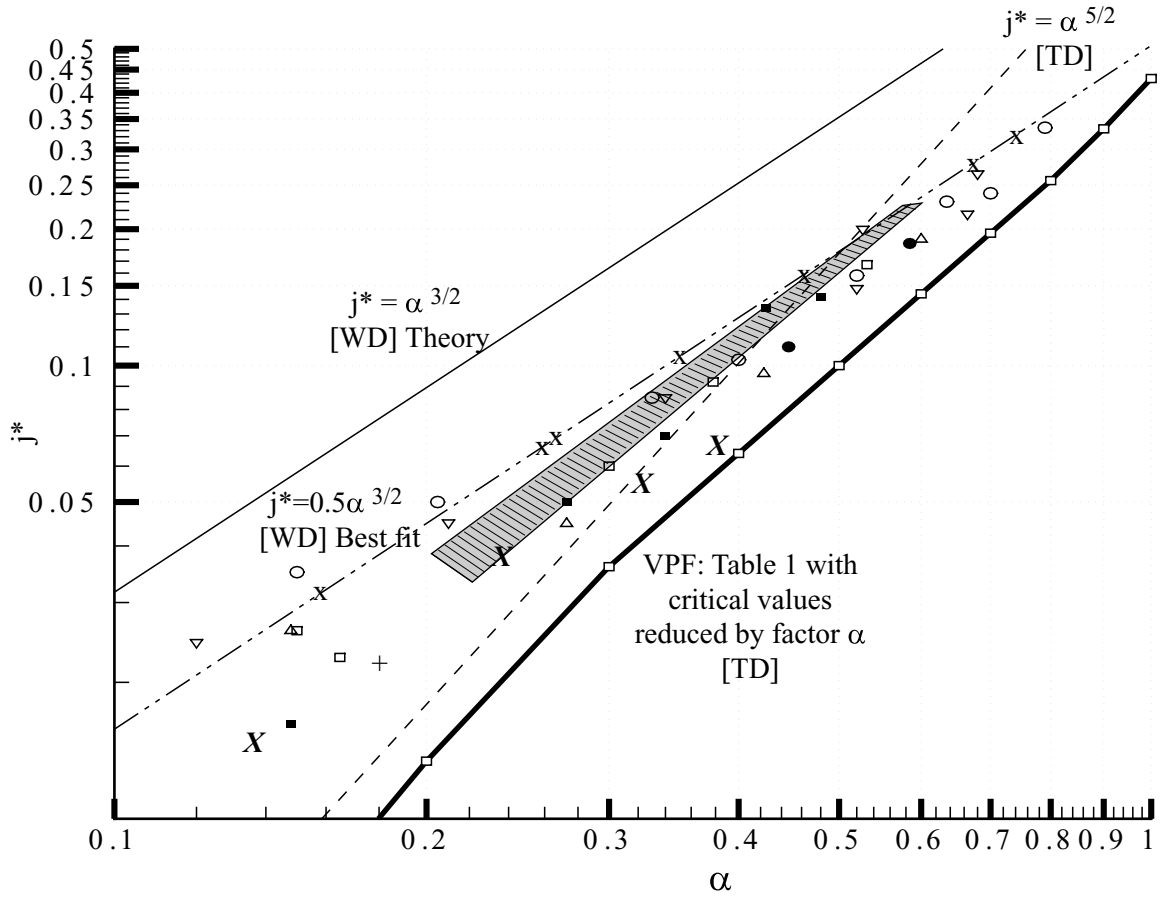

Figure 12: *Nonlinear effects. The Taitel-Dukler 1976 correction (multiply by α).*

Acknowledgements

This work was supported by the National Science Foundation award number CTS-0076648 and by the Army Research Office DA/DAAG55-98-1-0314.

List of Symbols

a	coefficient of the quartic equation; a_4, a_3, a_2, a_1, a_0
A_a, A_l, A_0	complex amplitudes for air, liquid and surface elevation
A, B, C	complex coefficients of the quadratic equation, $B = B_R + \imath B_I$ and $C = C_R + \imath C_I$
$\tilde{C}$	complex wave speed, $\tilde{C} = \tilde{C_R} + \imath \tilde{C_I}$
D	complex number, $D = D_R + \imath D_I$
e	strain tensor
g	acceleration due to gravity
h	height of a layer; h_a is the height of air layer, and h_l is the height of liquid layer
H	whole height of channel
$\imath$	$\imath = \sqrt{-1}$
j	flux
k	wavenumber
ℓ	the metric of interface deformation
p	pressure
Q	measure of velocity
t	time
u, w	velocity components of x and z
U	uniform velocity of x component
V	relative velocity defined by $V \equiv U_a - U_l$
x, z	components of the Cartesian coordinates
α	void fraction, $\alpha = h_a/H = \hat{h}_a$
γ	surface tension
Δ	horizontal Laplacian
θ	the growth rate parameter
λ	wave length
μ	viscosity
ρ	density
σ	complex growth rate, $\sigma = \sigma_R + \imath\sigma_I$
τ	viscous stress
ϕ	velocity potential
ω	complex frequency, $\omega = \omega_R + \imath\omega_I$

Superscripts

(a)	subscript for air
(l)	subscript for water

Subscripts

a	suffix for air
c	critical values of stability
C	values at cut-off wavenumber
I	imaginary part
l	suffix for liquid
m	values at maximum growth rate
R	real part
s	values taken at $k = 10^{-3}$[1/cm]
w	suffix for water
$\hat{}$	dimensionless quantity
$\tilde{}$	wave velocity

References

AH Andritsos, N. and Hanratty, T.J. 1987. Interfacial instabilities for horizontal gas-liquid flows in pipelines, *Int. J. Multiphase Flow* **13**, 583-603.

AWH Andritsos, N., Williams, L. and Hanratty, T.J. 1989. Effect of liquid viscosity on the stratified-slug transition in horizontal pipe flow. *Int. J. Multiphase Flow* **15**, 877-892.

B Barnea, D. 1991. On the effect of viscosity on stability of stratified gas-liquid flow – application to flow pattern transition at various pipe inclinations. *Chem. Engng. Sci.* **46**, 2123-2131.

BT Barnea, D. and Taitel, Y. 1993. Kelvin-Helmholtz stability criteria for stratified flow: viscous versus non-viscous (inviscid) approaches, *Int. J. Multiphase Flow* **19**, 639-649.

CWB Crowley, C.J., Wallis, G.B. and Barry, J.J. 1992. Validation of a one-dimensional wave model for the stratified-to-slug flow regime transition, with consequences for wave growth and slug frequency. *Int. J. Multiphase Flow* **18**, 249-271.

JBB Joseph, D.D., Belanger, J. and Beavers, G.S. 1999: Breakup of a liquid drop suddenly exposed to a high-speed airstream. *Int. J. Multiphase Flow* **25**, 1263-1303.

JL Joseph, D.D. and Liao, T. 1994. Potential flows of viscous and viscoelastic fluids. *J. Fluid Mech.* **265**, 1-23.

JLF Joseph, D.D., Lundgren, T.S. and Funada, T. 2000. Viscous Potential Flow Analysis of Kelvin-Helmholtz Instability. submitted to *Physics of Fluids.*

JR Joseph, D.D. and Renardy, Y.Y. 1991. *Fundamentals of two-fluid dynamics*, Chapters IV-VIII, Springer-Verlag, IAM 4.

JS Joseph, D.D. and Saut, J.-C. 1990. Short wave instabilities and ill-posed problems, *Theoretical and Computational Fluid Mechanics* **1**(4), 191-228.

KR Kordyban, E.S. and Ranov, T. 1970. Mechanism of slug formation in horizontal two-phase flow. *Trans. ASME J. Basic Engng.* **92**, 857-864.

LH Lin, P.Y. and Hanratty, T.J. 1986. Prediction of the initiation of slugs with linear stability theory. *Int. J. Multiphase Flow* **12**, 79-98.

TD Taitel, Y. and Dukler, A.E. 1976. A model for predicting flow regime transitions in horizontal and near horizontal gas-liquid flow. *AIChE J.* **22**, 47-55.

MI Mishima, K. and Ishii, M. 1980. Theoretical prediction of onset of horizontal slug flow. *Trans. ASME J. Fluids Engng.* **102**, 441-445.

W Wallis, G.B. 1969. *One-dimensional Two-phase Flow.* McGraw-Hill, New York.

WD Wallis, G.B. and Dobson, J.E. 1973. The onset of slugging in horizontal stratified air-water flow. *Int. J. Multiphase Flow* **1**, 173-193.

WPHM Wu, H.L., Pots, B.F.M., Hollenberg, J.F. and Meerhoff, R. 1987. Flow pattern transitions in two-phase gas/condensate flow at high pressure in an 8-inch horizontal pipe. 3-rd International Conference on Multi-phase Flow, The Hague, The Netherlands, Paper A2, 13-21.